

The unicellular NUM v.0.91: A trait-based plankton model evaluated in two contrasting biogeographic provinces.

Trine F. Hansen^{1*}, Donald E. Canfield^{1,2,3}, Ken H. Andersen⁴, Christian J. Bjerrum⁵

¹Nordcee, Department of Biology, University of Southern Denmark, Odense M, Denmark

5 ²Danish Institute of Advanced Studies (DIAS)

³Petrochina, Beijing, China

⁴Center for Ocean Life, National Institute of Aquatic Resources, Technical University of Denmark, Kongens Lyngby, Denmark

⁵Department of Geosciences and Natural Resource Management, University of Copenhagen, Copenhagen, Denmark

10

*Now at Center for Ocean Life, National Institute of Aquatic Resources, Technical University of Denmark, Kongens Lyngby, Denmark

Correspondence to: Trine F. Hansen (trfri@aqua.dtu.dk)

15 Abstract

Trait-based models founded on biophysical principles are becoming popular in planktonic ecological modeling, and justifiably so. They allow for slim, efficient models with a significant reduction in parameters, well suited for modeling the past and future climate changes. In their ~~simplest-idealized~~ form, trait-based models describe the ecosystem in one set of parameters defined by first principles, rooted in physics, chemistry, geometry, and evolution. The result is an emerging ecosystem defined by physical and chemical limitations at the cell level. At present, however, a significant part of these parameters is not fully constrained, which potentially introduces ~~a-considerable~~considerable uncertainty to the model results. Here, we investigate how these parameters influence the ecosystem structure of one of the simplest trait-based models, the Nutrient-Unicellular-Multicellular (NUM) model. We describe the unicellular module of the NUM model and through an extensive parameter sensitivity analysis, we demonstrate that the model - with a large span in parameters - can capture the general features of the pico-, nano-, and micro planktonic ecosystem ~~at-in the southern-California-Currenta high-productivity upwelling system~~. We ~~show-demonstrate~~ that it is possible to narrow the range of parameters to get a stable, acceptable, solution. Finally, ~~the we-show-thatmodel -the-model-~~responds correctly in an oligotrophic downwelling system using parameters fitted to the upwelling systemto-a-change-in-oceanographic-setting. Our analysis demonstrates that the unicellular module of the NUM model is broadly accessible ~~for the general non-expert~~ without ~~detailed intimate~~ knowledge of the parameter settings, and that the first-principal approach is well suited for modeling poorly resolved region and ecosystem evolution during current and deep time climate change.

25
30

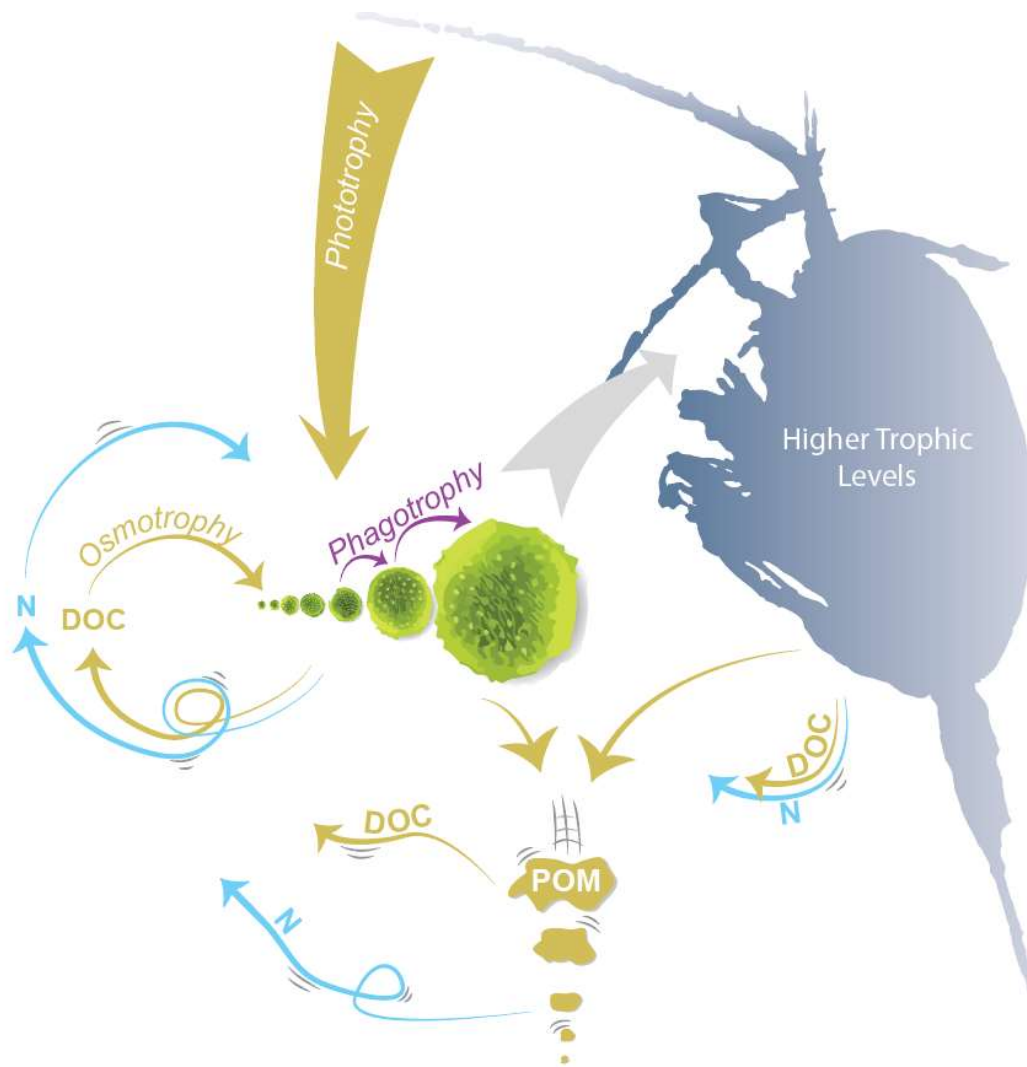
1 Introduction

Trait-based models are becoming an important tool for understanding the spatial and temporal pattern in planktonic ecosystem structure (e.g. Follows et al., 2007; Dutkiewicz et al., 2021; Ward et al., 2019; Eckford-Soper et al., 2022). Rooted in first principles of biophysics and biochemistry, trait-based models alleviate many of the caveats that confine traditional functional planktonic ecosystem models: they allow for large-scale ocean domains without the need for adding increased complexity; they reduce the amount of parameter tuning; and they allow for modeling evolution in the past and future, under climate change where ecosystems are different from the ones we know today (Reinhard et al., 2020; Sauterey et al., 2017; Wilson et al., 2018; Archibald et al., 2022).

There ~~is~~are a variety of approaches to trait-based modeling. For most of the trait-based planktonic ecosystem models, size is used as a master trait, as it scales with many of the cells processes and rates (Ward et al., 2019; Sauterey et al., 2015; Andersen et al., 2015). One particularly simple size-based plankton model is the Nutrient-Unicellular-Multicellular (NUM) model (Andersen and Visser, 2023; Serra-Pompei et al., 2020; Serra-Pompei et al., 2022). The NUM model is founded in the biophysical and chemical processes of the cell, scaled up to community level (Fig. 1). With the cell processes at the center, the result is a simple and fast model where size-spectrum and rates of photosynthesis, as well as uptakes of nutrients, dissolved organic carbon (DOC) and food (phagotrophy), emerges from the specific physical conditions of the oceanographic conditions (Andersen and Visser, 2023; Serra-Pompei et al., 2020).

Despite the simplicity of the NUM model, it - like any other model - relies ~~on~~ a set of parameters (Table 1). In principle, these parameters are universal and common for all organisms; however, they are not all well established. Some parameters are well defined by cell physiology, e.g., the maximum diffusive nutrient affinity coefficient (α_D) that is limited by cell surface area, but many have a range of uncertainty that emerges from natural cell variability or from a limited understanding of the parameter. As with any model, the output of the NUM model reflects the parameter choices. It is still, however, unclear how much the parameters influence the result, how much tuning the model ~~re~~require and how well the model transfers between sites with the current parameter uncertainty.

In this article we describe the unicellular module of the NUM model and evaluate the model's ability to capture well-established key ecosystem descriptors, its robustness, geographical transferability, and the relative importance of the underlying parameters. Specifically, we start by evaluating the model's ability to capture the size structure of the planktonic biomass at the California Current Ecosystem (CCE) (California-Current-Ecosystem-Lter and Landry, 2019; Taylor and Landry, 2018), ~~using default model parameters~~. Hereafter we ~~address the parameters, evaluate~~ how ~~the their-parameter uncertainty distributions~~ effects the ~~result, and how much sensitivity they add to the~~ model ~~sensitivity~~. We conclude by applying the identified optimal parameter values for the CCE in a test of the model's geographical transferability to the ALOHA station north of Oahu, Hawaii (Pasulka et al., 2013; Taylor and Landry, 2018).



65

Figure 1: Schematic of the unicellular module of the Nutrient-Unicellular-Multicellular (NUM) model. The unicellular organisms are here represented by 7 size-classes of organisms that can all get their nutrients and carbon from osmo-, photo- and phagotrophy. The uptake rates depend on the biophysics of the cell and the environmental availability of dissolved organic carbon (DOC), nutrient (N), light and food ~~availability~~ (smaller cells). Higher trophic levels are here parameterized as feeding on a specific size range of cells. Exudation, viral lysis, assimilation losses, and higher trophic level losses replenish the nutrients and carbon. Losses from sloppy feeding by phagotrophy and higher trophic level are re-introduced as particulate organic matter (POM) that sinks down through the water column and is remineralized into DOC and N. The model formulations are listed in Supplement S1.

75

80 **Table 1: Parameters used in this study. Reference values are based on arguments from Andersen and Visser (2023) and standard values used in the NUM model setup.**

Parameter		Unit	reference value	Parameter range		Parameter confidence ⁴
				min	Max	
carbon density	ρ	$\mu\text{gC } \mu\text{m}^{-3}$	0.4×10^{-6}	0.3×10^{-6}	0.5×10^{-6}	<u>1</u>
C:N mass ratio	$\rho_{\text{C:N}}$	gC gN^{-1}	5.68	2.7	8.7	<u>1</u>
Cell rate parameters						
Diffusive affinity coefficient	α_{D}	$\text{l } \mu\text{m}^2 \text{d}^{-1} (\mu\text{gC})^{-1}$	0.972	0.75	1.3	<u>1</u>
Diffusive affinity crossover	r^*_{D}	μm	0.4	0.1	5	<u>1</u>
Light affinity coefficient	α_{L}	$(\text{d } \mu\text{mol m}^{-2} \text{s}^{-1})^{-1} \mu\text{m}$	0.3	0.05	1.5	<u>2</u>
Light affinity crossover	r^*_{L}	μm	7.5	2.5	20	<u>2</u>
Light uptake efficiency	ϵ_{L}	unitless	0.8	0.1	0.9	<u>2</u>
Clearance rate	a_{F}	$\text{l d}^{-1} \mu\text{gC}^{-1}$	1.8×10^{-2}	8.23×10^{-4}	0.4455	<u>2</u>
Max. phagotrophic coefficient	c_{F}	$\mu\text{m d}^{-1}$	30	10	50	<u>3</u>
Assimilation efficiency	ϵ_{F}	unitless	0.8	0.1	0.9	<u>1</u>
Passive losses coefficient	c_{passive}	unitless	0.03	0.01	0.1	<u>2</u>
Maximum synthesis coef.	α_{max}	d^{-1}	1.5	0.1	2.1	<u>2</u>
Basal metabolism coef.	α_{R}	unitless	0.1	0.045	0.22	<u>2</u>
Prey encounter						
predator-prey mass ratio	β	unitless	500	300	700	<u>2</u>
predator-prey width	σ	unitless	1.3	0.9	1.7	<u>2</u>
community model parameter						
DOC remineralization-remin. of feeding	γ_{F}	unitless	0.1	0.1	0.9	<u>3</u>
DOC remineralization-remin. of viral lysis	γ_2	unitless	0.5	0.1	0.9	<u>3</u>
Viral lysis mort. coefficient	μ_{v0}	unitless	4.0×10^{-3}	4.0×10^{-4}	4.0×10^{-2}	<u>3</u>
Size of HTL mortality ¹	m_{HTL}	μgC	0.1	0.001	0.1	<u>2</u>
HTL mortality coefficient	μ_{htl}	d^{-1}	0.1	1.0×10^{-2}	0.25	<u>3</u>
Particulate organic matter (POM)						
POM sinking coefficient ^{3,2}	v_{I}	m d^{-1}	400 100	1	200	<u>2</u>
Inverse solubilization length scale ²	a	m^{-1}	0.004	0.002	0.006	<u>2</u>
Fraction of HTL mort. to POM	γ_{HTL}	unitless	0.5	0.1	0.9	<u>2</u>
Fixed parameters						
Membrane thickness	δ	nm	50			<u>2</u>
Light attenuation by water	k_{w}	m^{-1}	0.05			<u>2</u>
Light attenuation by POM ³	k_{POM}	$\text{m}^2 \text{mg C}^{-1}$	3×10^{-5} -	3×10^{-5}	3×10^{-5}	<u>2</u>
POM sinking exponent ³	v_2	md^{-1}	0.5130.2	0.2	0.2	<u>2</u>

¹The size of HTL mortality is between 100 and 10000 times smaller than the largest cell size.

²Fennel et al. (2001)

³POM was not included in previous versions of the NUM model and the parameters written in the reference value signify the values used in the initial evaluation of the model. Based on arguments in supplement S1, a k_{POM} value of $3 \times 10^{-5} \text{ m}^2 \text{ mg C}^{-1}$ is used for all simulations in this article. The choice in POM sinking coefficient and exponent result in a sinking speed of $0.01\text{-}3 \text{ m day}^{-1}$ for the smallest POM size classes and $1\text{-}200 \text{ m day}^{-1}$ for the largest, using the formulation for POM sinking in supplement S1.

⁴Qualitative parameter uncertainty ranging between 1 (low) and 3 (high) cf. Andersen and Visser (2023). Parameter uncertainty stem from limited understanding of processes and/or empirical evidence.

2 Model description

2.1 The Nutrient-Unicellular-Multicellular model framework

The NUM model is built on an additive model framework that relies on formulations of the fundamental properties of the organism (Andersen and Visser, 2023; Serra-Pompei et al., 2020; Serra-Pompei et al., 2022). The NUM model initially included copepods and protists as the unicellular and multicellular components of the model, along with nutrient (N) and fecal pellets (Serra-Pompei et al., 2020). Serra-Pompei et al. (2020) implemented the model in MATLAB with a chemostat setup. Later, Serra-Pompei et al. (2022) coupled the NUM model to a transport matrix, enabling both water column and global simulations. In a major update of the NUM model that resulted in the current version, where the core NUM model was translated from MATLAB to FORTRAN95. The model can be run directly from FORTRAN but can also be initialized from MATLAB and from R, which opens the model to users without FORTRAN experience. In this update, the NUM framework was extended to include a DOC module and a particulate organic carbon (POM) module.

The NUM model can be used in three different setups; It can be used in a global simulation where the NUM model is coupled to a transport matrix that provide advection, diffusion, and temperature for the simulation (Khatiwala, 2007); It can be used in a chemostat setup with a constant mixing rate and deep nutrient concentration; and finally, as we do here, it can be used in a water column simulation where temperature and diffusion at single location is extracted from the transport matrix. Here, we describe and evaluate the unicellular organisms and the particulate matter, and we will therefore limit the description of the NUM framework to these parts. The model formulations are provided in Supplement S1. Section 2.2 describes the unicellular module and parameters while section 2.3 describes the new simple DOC and POM modules and the associated parameters.

2.2 The unicellular module

The backbone of the NUM is the unicellular module that ~~comprise~~comprises the classic functional groups of phytoplankton, osmotrophic bacteria, and zooplankton. While unicellular organisms span many orders of magnitude in size, across all types of trophic strategies (feeding mechanisms), they are all described with one set of parameters in the unicellular subroutine of NUM. Here, the cell may be visualized as one type of organism – we refer to as a *generalist* - that is essentially a mixotroph in the sense that it is able to perform osmotrophy (diffusive uptake of DOC), photosynthesis and phagotrophy (food consumption) to gain nutrient and carbon. The generalist can utilize all three trophic strategies at the same time. However, the yield from each of these strategies depends on the size of the generalist and on the surrounding environmental conditions (light level, nutrient and dissolved organic carbon concentration, food, etc.). The model contains several of these generalists with the only difference being the size of the organism, defined in logarithmic size-bins of mass, m . The output of the generalist subroutine is the biomass of each of the generalist size bins and the associated rates of phototrophy (J_{auto}), osmotrophy (J_{osmo}) and phagotrophy (J_{phag}). This approach makes the unicellular module especially well adapted to handle mixotrophic organisms. In the following subsections, we will go through the most important processes controlling the generalist growth and, size structure ~~and the formation of particulate organic matter (POM)~~. The aim of this section is to give the reader an understanding of the mechanisms that control the organism and a sense of the parameters that are evaluated in this study. The important parameters are highlighted in bold in the text below. The following sections summarize the more detailed description of the model given in Serra-Pompei et al. (2020) and Andersen and Visser (2023).

2.2.1 Resource uptake

The organism's affinity for (*meaning its ability to take up*) dissolved organic matter and nutrients (a_D), light (a_L) and for food phagotrophy (a_F) is dependent on its size. The affinities for uptake of these resources are determined by the encounter rate (*how much resource the generalist is in contact with*) and the assimilation rate (*how fast it can take up the resource it encounters*).

The affinity for diffusive uptake of nutrients and dissolved organic carbon (DOC) is modeled as a crossover between two size regimes: large and small organism size. For large organisms, the limiting factor is the rate of diffusion towards the outer cell membrane. In contrast for smaller organisms, it is the numbers of cell porter channels that transport the resource across the cell membrane (Eq. (1), all equations referred to are listed in Table 2). The parameter r^*_D determines the organism size where the crossover between the two regimes ~~occur~~occurs, and the diffusive affinity coefficient, α_D , defines the upper limit of the diffusive encounter.

The affinity for uptake of carbon through photosynthesis, a_L , is also modeled as a crossover between two regimes (Eq. (2)). For small organisms a_L is dependent on the organism's mass, while for larger organisms, where light harvesting complexes create internal shading, a_L is dependent on the cell surface area. The parameter r^*_L determines the crossover size between the two regimes. The parameter α_L is defined as $\alpha_L = 3\gamma/(4\rho)$, where γ is the quantum-yield (describing the efficiency of the

process relative to the available photons) and ρ is the carbon density of the individual cell (cf. Andersen and Visser, 2023).

145 The light uptake efficiency (ϵ_L) is a fraction that defines how efficient the organism is at utilizing the available light.

Phagotrophy is modelled as a hyperbolic curve where an increase in the amount of prey ingested increase with the prey density, until saturation of prey ingestion occurs. Such ecological type-II functional response has a constant affinity (the clearance rate, α_F) and a maximum assimilated phagotrophic uptake that is dependent on the assimilation efficiency (ϵ_F) and the maximum phagotrophic coefficient (c_F) (Eq. (3)).

150 2.2.2 Synthesis, respiration, and losses

The generalist might be able to take up more nutrient and carbon than it is able to synthesize. The rate of biosynthesis is controlled by the maximum synthesis coefficient (α_{max} , Eq. (4)). Nutrients and carbon in excess leaks out of the cell. Beside the resource uptake, the organism passively leaks carbon and nutrients through the cell membrane. This process is modeled as a constant, $c_{passive}$, divided by the radius of the organism (Eq. (5)). Finally, the organism's respiration rate is modeled as a

155 fraction of the maximum synthesis coefficient (Eq. (6)). This is called the basal metabolism coefficient, α_R .

2.2.3 Prey-predator interactions

The generalist is potential prey for two groups: other larger generalists and predators from higher trophic levels. The generalist's internal prey-predator relationship is based on the two parameters, β and σ (Eq. (7)). β defines the mean mass ratio between the prey and the predator. The parameter σ defines the wideness of the preferred size range that a predator prey

160 on. The mortality from higher trophic levels is likewise defined by two parameters: m_{HTL} , that defines the lower limit (expressed as mass) of organisms that are preyed upon by higher trophic levels, and the higher trophic level mortality coefficient, μ_{HTL} , that defines the rate of predation by higher trophic levels.

Lastly, the generalists undergo viral lysis. The rate is controlled by the parameter μ_{v0} and dependent on the logarithmic size bin length (Eq. (8))

165

2.2.43 Remineralization-Dissolved organic carbon and particulate organic matter

This version of the NUM Andersen and Visser (2023) incorporates both dissolved and particulate matter in a simplified approach (Fig. 1). Dissolved nutrients, both inorganic and organic N containing, are modelled as one dissolved N pool, while dissolved organic carbon (DOC) is modelled separately. The particulate matter (POM) contains both C and N in a fixed ratio. Dead cells, feeding losses, and higher trophic level mortality produce both particulate organic matter (POM) and dissolved constituents (DOC and N). Note, that the choice of pooling inorganic and organic N in a single pool means that the microbial consumption/remineralization of N is not explicitly resolved as dependent on osmotrophy. In contrast, consumption of DOC as an energy source for heterotrophic osmotrophy is explicitly modelled as presented above (section 2.2.1). The pool of DOC in this model represents "labile" DOC. The division between the particular and dissolved fractions

170

175 are determined by the γ parameters (γ_2 , γ_F and γ_{HTL}), which describe how much of each flux (mortality, feeding losses, and
higher trophic level mortality) are routed to the dissolved fractions, with the remaining losses transferred to POM. Particulate
organic matter is here divided into two different size fractions (a number that can readily be increased in future applications).
POM derived from dead cells and feeding losses is transferred to the largest POM size fraction, which is smaller than the
size of the original cell. POM from higher trophic level mortality is transferred into the largest POM size fraction. POM
180 sinks with a size-dependent velocity. Particulate organic matter (POM) and dissolved organic carbon (DOC) are a product of
cell mortality, feeding losses and higher trophic level mortality. Three parameters determine how much of the cell mortality
(γ_2), feeding losses (γ_F) and higher trophic level mortality (γ_{HTL}) are converted to nutrients and carbon. γ_2 , γ_F and γ_{HTL} can
vary between 0 and 1, with the remaining losses transferred into particulate organic matter. The sinking velocity of POM is
dependent on the size of particle, and it is described as a power function with the parameters v_1 and exponent v_2 (Eq. (9)).
185 POM is assumed to remineralize directly. Remineralization of detritus to the dissolved N and DOC pools. This process of
remineralization is not explicitly microbial cell related in the model but occurs at a constant rate determined by the inverse of
the solubilization length scale is modeled as a constant rate (a) as $rem_{POM} = aw_{POM} \cdot \gamma_{POM}$. The model formulation of
nutrient, along with DOC and POM modules are given in Supplement S1.

190

195

200

205 **Table 2: Equations used for the unicellular submodule. Full model description is given in Supplement S1.**

Affinity for nutrients and dissolved organic matter.	$a_D = \alpha_D r^{-2} \frac{1}{1 + (\frac{r}{r_D^*})^{-2}} m$	Eq.1
Affinity for carbon uptake through photons	$\alpha_L = \frac{\alpha_L}{r} (1 - e^{-\frac{r}{r_L}}) (1 - \nu) m$	Eq.2
Rate of phagotrophy	$J_F = \epsilon_F c_F r^{-1} \frac{a_F F}{a_F F + c_F / r} m$	Eq.3
Maximum biosynthesis rate	$J_{max} = \alpha_{max} (1 - \nu) m$	Eq.4
Passive losses	$j_{passive} = c_{passive} r^{-1}$	Eq.5
Respiration rate	$J_R = \alpha_R \alpha_{max} m$	Eq.6
Size preference for predation	$\varphi = \exp \left[- \frac{\ln^2 \left(\frac{m}{\beta m_{prey}} \right)}{2\sigma^2} \right]$	Eq.7
Viral lysis ¹	$\mu_v = \frac{\mu_{v0}}{\log \left(\frac{m^+}{m^-} \right)}$	Eq.8
Sinking of particulate organic matter	$w_{POM} = \nu_1 m^{\nu_2}$	Eq.9

¹ m^+ and m^- is mass of the upper and lower limit of the size bin

3 Modelling approach

In this article, we are using the water-column setup of the NUM model to simulate the conditions at the southern California Current Ecosystem (CCE) and Station ALOHA. We initially perform a general validation of the model with default parameters against the mean biomass size spectrum and nutrient profile for the two locations. The subsequent analysis is aimed at understanding the model's performance, robustness, transferability, and parameter sensitivity.

The investigation has two levels: an overall broad random parameter evaluation followed by three more detailed statistical sub-analyses.

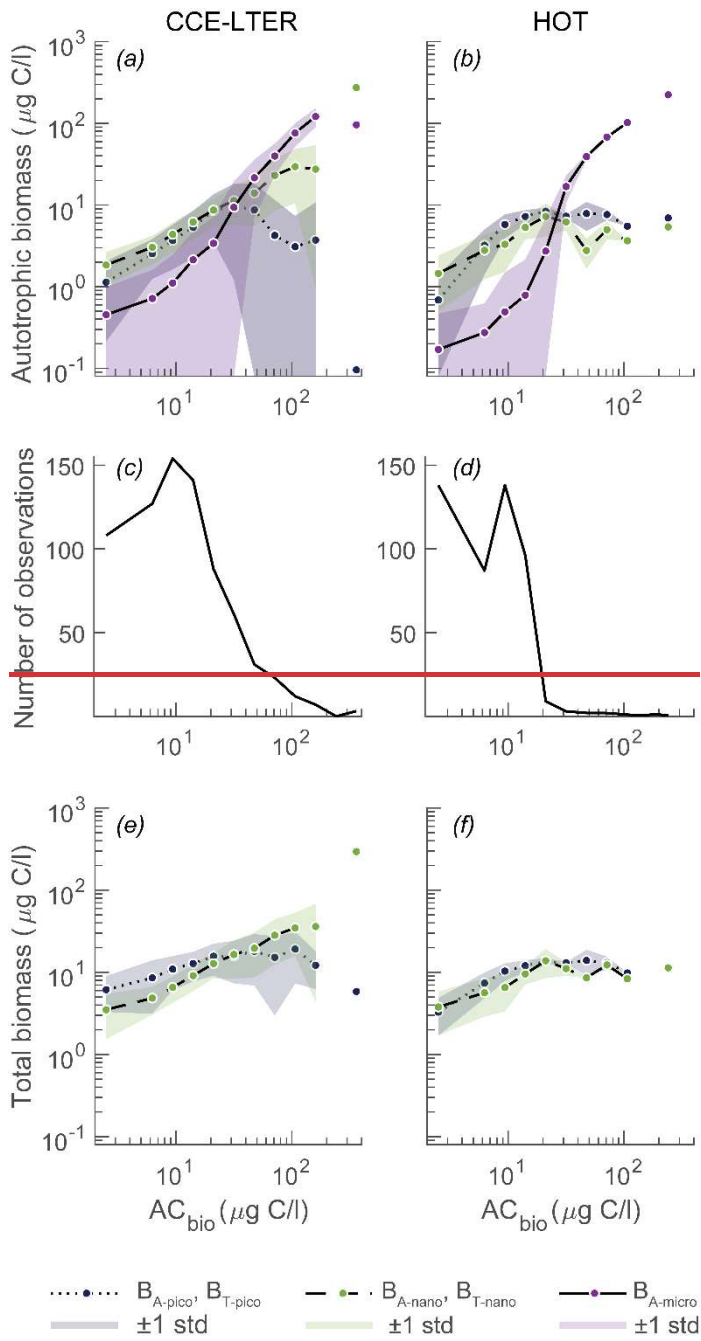
The first-level parameter study is comprised of 100,000 simulations with quasi-random input parameters in the range defined in Table 1. Of the 23 free parameters, several are assigned a span of several orders of magnitude, which is computationally demanding but enables a genuine investigation of the solution space and variability for the model. We use Latin hypercube sampling scheme for all 23 parameters to ensure an even spread in the entire parameter space (Mckay et al., 1979; Stein, 1987) and evaluate the model performance by comparing the results with observations, using a set of statistical

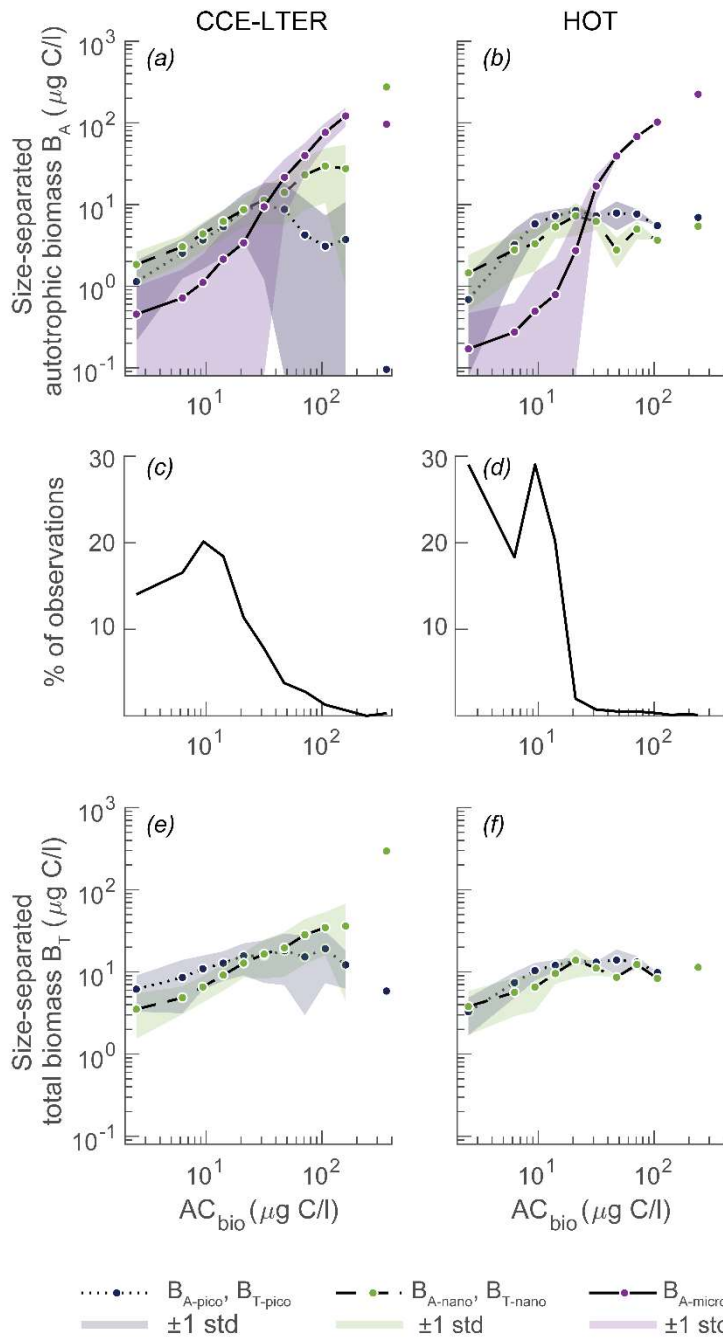
matrices that will be described below. We moreover use this first-level parameter study and evaluation to identify optimized parameter combinations that result in good model fit to CCE observations. These optimized parameter combinations define a *restricted parameter spans* that permit us to make three additional statistical subanalysis for CCE. The first subanalysis is a set of 10,000 simulations where input parameters are quasi-randomly sampled with the Latin hypercube sampling scheme within the *restricted parameter spans*. This subanalysis allow us to determine if only very specific combination of parameter results in good model fit or if how much model performance is increased by simply reducing the parameter span. The second subanalysis is a set of local sensitivity analyses where the model's sensitivity toward each of the parameters is evaluated separately with outset in an initial specific parameter combination (Zhou and Lin, 2008). The local sensitivity analysis is made with outset in the initial parameter combinations that performs outset in the seven best parameter combinations for CCE, where ~~e~~Each of the parameters are successively varied in 50 evenly distributed intervals within the *restricted parameter span*. This subanalysis showed that several of the parameters results in systems bifurcation points where the model solution changes abruptly. While being extremely interesting, the detailed analysis of such bifurcation points is beyond the current scope and remains a prospect for future analyses. The subanalysis also showed that most parameters are highly coupled in term of ecosystem sensitivity, where the effect of individual parameters are intertwined and result in a highly non-linier system. The sensitivity analysis with a specific parameter outset yielded nearly equally sensitive to almost all parameters whereas with a different parameter outset, ϵ_F was the absolute most important parameter. Because of these highly non-linier parameter interactions, local sensitivity studies give little added information about the model performance. We have added two of these seven tests in Supplement S4. The third subanalysis is a global variance-based sensitivity analysis using Sobol's method and sensitivity index (Bilal, 2014; Sobol, 1993, 2001). The global variance-based sensitivity analysis not only accounts for the effect of each individual parameter on the modeled result (the first-order effect) but also more interestingly, the effects of the parameter through its interactions with other parameters (total effect) (Bilal, 2014; Zhou and Lin, 2008). The global sensitivity analysis is made following Bilal (2014), as a set of 20,000 simulations with parameter combinations based on random sampling of the *restricted parameter spans*. Then, for each of the 20,000 simulations we step through the parameters and perform two simulations: (1) the parameter in question is kept at its value while the other 22 parameter are selected quasi-randomly within the restricted parameter span, and (2) the parameter in question is randomly selected in the parameter span while all other parameters are kept at their values (Bilal, 2014; Sobol, 2001). A step-by-step description for the process for setting up the global sensitivity analysis is included in Supplement S5.

The model evaluation and statistical test against the CEE permit us to identify seven optimized parameter combinations that result in a good model fit to observations for the CCE. We then finally evaluate how the model performs within the *restricted parameter spans* at Station ALOHA that, with is different physical and chemical conditions, represent an oligotrophic downwelling system. These results are evaluated against a first-level parameter study at ALOHA with 100,000 quasi-random parameter combinations.

3.1 Observational data

Compilations of the composition of phytoplanktonic communities have illuminated some systematic trend in the size distribution of planktonic organisms as a function of chlorophyll and autotrophic biomass concentration (AC_{bio}) (Taylor and Landry, 2018; Maranon et al., 2012; Ward et al., 2014). Analyses across various provinces in the Atlantic and in the North Pacific broadly reveal that, when chlorophyll a (Chl-*a*) or primary production is low, ~40% of the biomass is dominated by picophytoplankton (0.2–2 μm), irrespective of temperature. As Chl-*a* increases, microphytoplankton (>20 μm) increase in biomass and dominate when Chl-*a* is high. Nanophytoplankton (2–20 μm) is intermediate between pico- and microphytoplankton at both low and high Chl-*a*. Similar trends are present at sub-regional or local scale in detailed work that is described below (Taylor and Landry, 2018; Taylor et al., 2015; Goericke, 2011) (Fig. 2). Because of the apparent pervasiveness of these trends and characteristic of the planktonic community in marine ecosystems, size structure represents an excellent test for the model’s adaptability across oceanographic regimes.





265

Figure 2: Observed plankton biomass as function total autotrophic biomass (AC_{bio}). (a, b) Mean biomass of pico- ($< 2 \mu\text{m}$, B_{A-pico}), nano- ($2-20 \mu\text{m}$, B_{A-nano}) and microautotrophs ($> 20 \mu\text{m}$, $B_{A-micro}$) at (a) California current ecosystem (CCE) with upwelling, (b) Hawaii ocean time series (HOT) with downwelling conditions. Data are compiled from 0-200 m depth from 2004 to 2011 and has been binned in logarithmically distributed bins. (c, d) Number of observations per bin at respective sites. (e, f) Total picoplankton

270 (B_{T-pico}) and nanoplankton (B_{T-nano}) biomass, respectively at CCE and HOT, is the sum of autotrophic and heterotrophic biomass.
| ~~DD~~ Data and binning method from Taylor and Landry (2018) and references in text. Note that CEE relative to HOT is more
eutrophic reflected by more data in higher AC_{bio} bins (c vs. d).

Here, we compare the model result to size-spectrum data gathered from the southern California Current Ecosystem (CCE)
as a part of the California Current Ecosystem Long Term Ecological Research (CCE-LTER) and from Station ALOHA, the
275 long-term Hawaii Ocean Time series (HOT) (Taylor and Landry, 2018; Pasulka et al., 2013; California-Current-Ecosystem-
Lter and Landry, 2019) (Fig. 2). These two sites reflect distinctly different oceanographic regimes: coastal upwelling with
eutrophic conditions at CCE and downwelling oligotrophic open-ocean waters at Station ALOHA. Both sites have been
sampled for epifluorescence microscopy and flow cytometry regularly in the years 2004 to 2011, resulting in large datasets
of biomass abundance, size structure and planktonic composition. The phytoplanktonic size structure of the two sites show
280 many of the same features as the large-scale compilations of planktonic size distribution: Pico- and nano- autotrophic
organisms dominate the size spectrum at low autotrophic carbon biomass (AC_{bio}) where the concentrations of
microautotrophic organisms are very low (Fig. 2a, b) (Taylor and Landry, 2018; Maranon et al., 2012; Ward et al., 2014).
The concentration of all three size classes increases with increasing AC_{bio}, however, the autotrophic microplankton
concentration increases faster than the smaller size groups and become dominant at intermediate levels of AC_{bio}
285 (approximately 20 µgC l⁻¹). Microautotrophic plankton continue to increase in a power law fashion for both observational
datasets. In contrast, the pico- and nanoautotrophs increase as a function of AC_{bio} is different at the two sites. The CCE-
LTER dataset ~~follow~~follows the global tendency of a continued increase in nano-autotrophs while the pico-autotrophs
decrease toward high AC_{bio}. The HOT observations show a steadier concentration for both pico- and nanoautotrophs across
AC_{bio} concentrations, but with a small decrease in nanoautotrophs at high AC_{bio}. ~~OverallWhile~~, the two sites show many of
290 the same features, ~~but~~ we note that high autotrophic biomass concentrations are much more frequently observed at CCE than
at Station ALOHA (Fig. 2, c-d). However, it is only in approximately two percent of the observations from the CCE-LTER
dataset that autotrophic biomass has been measured as high as 100 µgC/l. At Station ALOHA, only four percent of the
observations has autotrophic biomass concentrations of 30 µgC/l.

As explained above, the unicellular subroutine of the NUM framework calculates the rate of nutrient and carbon uptake
295 J_{auto} , J_{osmo} , and J_{phago} for each generalist size bin, while the specific trophic strategy is not explicitly calculated. The
observations of autotrophic organisms in the CCE-LTER and HOT datasets are on the other hand based on the presence of
chlorophyll-*a* in ~~epifloureseeneepifluorescence~~ epifluorescence microscopy as well as on DNA and photosynthetic pigments in flow
cytometry. In these types of analysis, an organism is either classified as autotroph or heterotroph with no room for
distinguishing degrees of mixotrophy. It therefore requires a post-processing of our model result to be able to compare with
300 observations. Our processing approach is described below. To minimize the significance of the uncertain distinction of
mixotrophy in comparison with observations, we also calculate the total biomass (heterotrophic plus autotrophic carbon) of
the pico- and nano-sized classes (Fig. 2 e-f). The addition of the heterotrophic component increases the overall biomass of
pico- and nanoplankton, especially in the CCE-LTER observations, but has very little influence on the overall size-

distribution of the plankton. Finally, we do not calculate the total biomass in the micro-sized bin, as observations in this size class are significantly underestimated (Taylor et al., 2011). Taylor et al. (2011) finds that micro-sized heterotrophic ciliates are poorly preserved in the epifluorescence slide-making protocol.

3.2 Evaluation metrics

The model result size spectrum is recalculated into different pools of biomass carbon (Table 3): The sum of heterotrophic and autotrophic biomass size classes is referred to as total picoplankton ($B_{T\text{-pico}}$) and total nanoplankton ($B_{T\text{-nano}}$). The autotrophic biomass in the size classes is referred to as autotrophic picoplankton ($B_{A\text{-pico}}$), autotrophic nanoplankton ($B_{A\text{-nano}}$) and autotrophic microplankton ($B_{A\text{-micro}}$). These different biomass classes are calculated for each autotrophic biomass bins (AC-bins) the same way that Taylor and Landry (2018) processed they observations (Fig. 2).

Table 3: Notation used for different biomass size classes

<u>Notation</u>	<u>Biomass class</u>	<u>Size range</u>
$B_{T\text{-pico}}$	<u>Biomass of total picoplankton</u>	<u><2 μm</u>
$B_{T\text{-nano}}$	<u>Biomass of total nanoplankton</u>	<u>2-20 μm</u>
$B_{A\text{-pico}}$	<u>Biomass of autotrophic picoplankton</u>	<u><2 μm</u>
$B_{A\text{-nano}}$	<u>Biomass of autotrophic nanoplankton</u>	<u>2-20 μm</u>
$B_{A\text{-micro}}$	<u>Biomass of autotrophic microplankton</u>	<u>20-200 μm</u>

To calculate how much of the model biomass should be classified as autotrophic we first define two ratios $\gamma_{A:F} = J_{\text{auto}} / (J_{\text{auto}} + J_{\text{phago}})$ and $\gamma_{A:O} = J_{\text{auto}} / (J_{\text{auto}} + J_{\text{osmo}})$, where J 's are the different rates of carbon synthesis defined above. If the ratio $\gamma_{A:F}$ is above 0.1, we classify the generalist in that size bin as a fully photoautotrophic organism for comparison with observations (Stoecker et al., 1996; Stukel et al., 2011). We then calculate the autotrophic biomass in that size bin(i) based on the combined rates of autotrophic and phagotrophic biosynthesis as:

$$B_{\text{auto},i} = B_i \frac{J_{\text{auto},i} + J_{\text{phago},i}}{J_{\text{auto},i} + J_{\text{phago},i} + J_{\text{osmo},i}}$$

If $\gamma_{A:F}$ is below 0.1, we instead define that the generalist in that size bin is both auto- and **phagotrophphagotrophic** and the autotrophic biomass is calculated as:

$$B_{\text{auto},i} = B_i \frac{J_{\text{auto},i}}{J_{\text{auto},i} + J_{\text{phago},i} + J_{\text{osmo},i}}$$

The same philosophy is used for the osmotrophic-autotrophic ratios.

While the use of $\gamma_{A:F}$ is inspired by red/green fluorescence ratio (~0.08) used to partition mixotrophic nanoplankton into functionally phototrophs or heterotrophs in observational datasets (Stukel et al., 2011), we test our results for a range of values (0.1 –0.9) and find that this range does not change our results quantitatively.

In evaluating our model against observations, we use oceanographic statistical practice as described in Taylor (2001). For each of the 14 AC-bins we first calculate the mean and ~~its~~ standard deviation (STD) for the model and for the observations over the years of 2004-2011. Based on these means and STDs we then calculate the model versus observation correlation coefficient (COR_{m-o}), root-mean square difference ($RMSd_{m-o}$) as well as centered root-mean square error ($cRMS_{m-o}$) for the 14 AC-bins (Table 4). ~~The statistical~~Statistical comparisons are only made between model and observation AC-bins if there are more than two observations in an AC-bin. The model-observation comparison is based on the upper 100 meters of water columns because this increases the total number of observations through the year. Taylor and Landry (2018) evaluated only the upper 30 meters of their observations. Our reanalysis of their data shows no significant change in the observed distribution of pico-, nano-, and microautotrophic organism relative to their results, when we also include observation between 30 and 100 m.

The statistical measures are objective, but we need to ~~identify-define~~ what ~~is~~ acceptable model results are. We work with the premises that we cannot expect to have a better fit to the mean observation (mean of 2004-2011) than the year-to-year variation that is observed at the specific site. For each year between 2004-2011 ~~W~~we therefor calculate annual means and ~~its~~ standard deviation~~STDs~~ for each AC-bin based on the observations ~~from 2004 to 2011~~(STD_{ia} , Table 4). We refer to differences from year to year as the inter-annual variation in observations. We then evaluate correlation coefficient and root-mean-square difference between the annual mean observation and the total mean observation for all 14 AC-bins (abbreviated COR_{iao} and $RMSd_{iao}$, respectively. Notice the difference from the subscripts above). These statistics ~~informs~~inform us how much natural variation occurs around the mean observation. The minimum COR_{iao} and maximum $RMSd_{iao}$ of the inter-annual variation is used to determine if a model result is successful (COR_{iao} and $RMSd_{iao}$ values are available in Supplement S2). For example, if the correlation coefficient of the model average versus the observed total mean is higher than the correlation coefficient of the inter-annual variation ($COR_{m-o} > COR_{iao}$) then the model result for a given parameter set is considered successful in terms of correlation coefficient. Ideally, the optimal successful model simultaneously has $COR_{m-o} > COR_{iao}$ and $RMSd_{m-o} < RMSd_{iao}$ for all biomass size categories. As is clear below, no model results fulfill both criteria for all biomass size categories. Instead, we isolate the model results that fit the COR and RMSd criteria for at least 8 out of 10 size categories and has biomass in AC_{bio} -bin up to at least $40 \mu gCl^{-1}$ for CCE and $15 \mu gCl^{-1}$ for HOT. For the solutions that fulfill these criteria we sort them according to their COR_{m-o} and $RMSd_{m-o}$ and make a visual qualitative assessment in comparison with observations (cf. Fig 2).

Table 4: Definitions of biomass metrics and their calculations

Metric	Description	Formula
STD_o^1	Standard deviation of observed biomass (o) across AC _{bio} -bins (N), calculated from the mean biomass (\bar{o}) values.	$std_o = \sqrt{\frac{\sum_{n=1}^N (o_n - \bar{o})^2}{N}}$
STD_{ia}^2	Standard deviation of biomass for a given year (o_{ia}) for each AC _{bio} -bins (N), showing inter-annual variability.	$std_{ia} = \sqrt{\frac{\sum_{n=1}^N (o_{ia.n} - \bar{o})^2}{N}}$
STD_m	Standard deviation of modelled biomass (m) across AC _{bio} -bins (N), calculated from the mean modelled biomass (\bar{m}) values.	$std_m = \sqrt{\frac{\sum_{n=1}^N (m_n - \bar{m})^2}{N}}$
COR_{m-o}	Correlation coefficient between modelled biomass and mean observed biomass for each AC _{bio} -bins (N)	$COR_{mo} = \frac{\sum_{n=1}^N (o_n - \bar{o})(m_n - \bar{m})}{N} \frac{1}{std_o std_m}$
COR_{iao}	Correlation coefficient between yearly observed biomass and mean observed biomass for each AC _{bio} -bins (N)	$COR_{iao} = \frac{\sum_{n=1}^N (o_n - \bar{o})(o_{ia.n} - \bar{o})}{N} \frac{1}{std_o std_{ia}}$
$cRMS_{m-o}$	Centered root-mean square difference between modelled biomass and mean observed biomass for each AC _{bio} -bins (N)	$cRMS_{mo} = \sqrt{\frac{\sum_{n=1}^N ((m_n - \bar{m}) - (o_n - \bar{o}))^2}{N}}$
$RMSd_{m-o}$	root-mean square difference between modelled biomass and mean observed biomass for each AC _{bio} -bins (N)	$RMS_{mo} = \sqrt{\frac{\sum_{n=1}^N (m_n - o_n)^2}{N}}$
$RMSd_{iao}$	root-mean square difference between yearly observed biomass and mean observed biomass for each AC _{bio} -bins (N)	$RMS_{iao} = \sqrt{\frac{\sum_{n=1}^N (o_{ia.n} - o_n)^2}{N}}$

¹*STD_o represents the variability of biomass among size classes within the dataset averaged across the years 2004 to 2011.*

370 *This is a mean of all data within the upper 100 meters for all sampling data and location and interannual variability is thus not present here.*

²*STD_{ia} captures how biomass in each size class for a given year deviates from the dataset averaged across the years 2004 to 2011.*

3.3 Initial- and boundary conditions

375 The analyses are performed in a water-column setup of the NUM model with vertical diffusion and temperature profiles for the two sites extracted from the global 1° transport matrix MITgcm_ECCO (Stammer et al., 2004). Light, expressed as PAR, is modeled according ~~with~~to daily insolation depending on the specific latitude, day of the year, and time of day. The NUM model uses nitrate as nutrient and is initialized with annual mean observations of nitrate concentrations based on data from CCE-LTER and HOT (Calcofi-Scripps-Institution-of-Oceanography and Wilkinson, 2022; Pasulka et al., 2013; Karl and
380 Lukas, 1996) The nitrate observations have been smoothed with a Gaussian filter to reduce noise. The observations from Station ALOHA only ~~includes~~include nutrient measurements to a depth of 175 meters. Mean nitrogen values from World Ocean Atlas 2018 are used below this depth (Garcia, 2018; Garcia et al., 2019).

The model is simulated with 10 logarithmically distributed size classes of generalists in the range from 3 pgC to 10 µgC, equivalent to a spherical cell diameter of approximately 0.25 µm to 363 µm. In addition to the 10 size classes of generalists,
385 the model has small and large detritus of particulate organic carbon with different sinking velocities. The model is run for 15 years with daily output. The last five years are averaged and evaluated to smooth out inter-annual differences in model results. DOC is initialized with a value of 60 µmol kg⁻¹ (Zakem and Levine, 2019; Sarmiento and Gruber, 2006; Letscher and Moore, 2015). *DOC rapidly decreases to dynamic steady state with an annual mean value of ~1 ± 0.5 µmol kg⁻¹.*

390 4 Results

4.1 Model validation

Initial simulations have shown that 15 years is sufficient to produce a *dynamic steady state with* steady annual cyclicality. Of the 100,000 simulations for CCE, less than 1% terminated due to instability generated by the combinations of parameters. Random sampling of the simulations that integrated properly (completed) showed results were reproducible in re-runs and
395 that the model had reached *dynamic* steady state.

To validate the model's first-order response, we simulated conditions for the California Current Ecosystem (CCE) and Station ALOHA using the reference parameters from Table 1. The results were then compared to observed biomass spectra and nitrogen depth profiles for the two sites (Fig. 3). The contrasting oceanographic regimes between the sites are evident from their nitrogen profiles (Fig. 3a, b). The California Current Ecosystem, characterized by coastal upwelling, shows a

400 nitricline at approximately 100 meters depth. In contrast, Station ALOHA, an oligotrophic open-ocean site with
downwelling, exhibits lower nitrogen levels and a deeper nitricline. The model responds correctly to the difference in
circulation at the two sites resulting in higher nitrogen concentration at CCE compared to Station ALOHA. Although the
model's results generally align with observations, there is a depressed nitricline at CCE, leading to lower-than-expected
nitrogen values in the upper 200 meters of the water column and slightly elevated nitrogen concentrations at Station
405 ALOHA.

Despite these differences in nitrogen profiles, the biomass size distributions at both sites are remarkably similar (Fig. 3c,
d). Both sites display a relatively flat Sheldon biomass spectrum, with a mean biomass of approximately 1 $\mu\text{gC/L}$ at CCE
and approximately 0.5 $\mu\text{gC/L}$ at Station ALOHA. These biomasses are within the expected range of observations, although
the mean observed biomass is slightly higher, averaging 1.5 $\mu\text{gC/L}$ at CCE and 0.5 $\mu\text{gC/L}$ at Station ALOHA. Notably, the
410 largest discrepancy between the model and observations occurs in the small size classes at Station ALOHA, where the model
underestimates the biomass. The larger standard deviations observed at CCE indicate a more variable environment compared
to Station ALOHA.

415

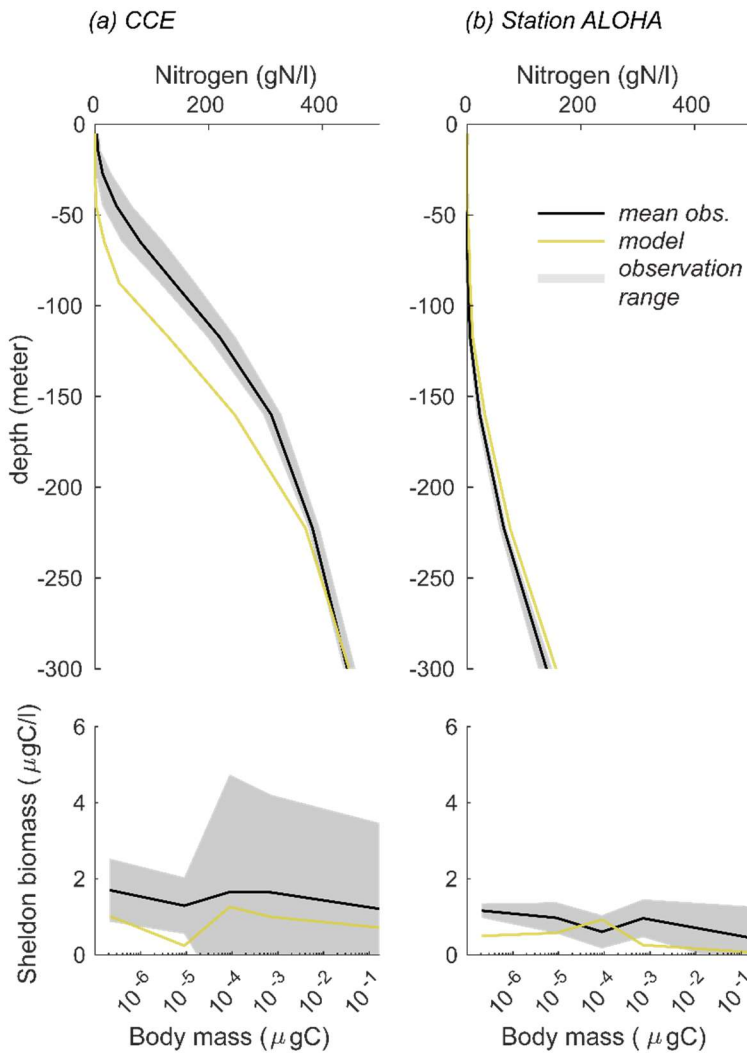


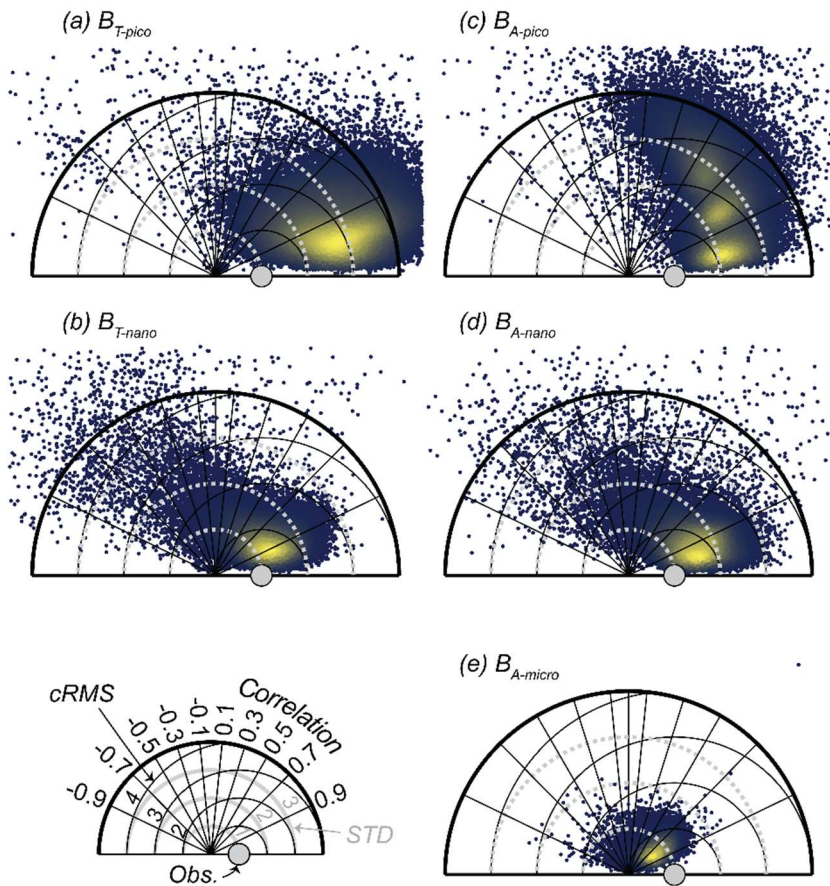
Figure 3: Nutrient profile and Sheldon biomass comparison between observations and reference model simulation for (a) CCE and (b) Station ALOHA. The Sheldon biomass spectrum illustrates the biomass in each body mass bin normalized with bin width. The

420 Sheldon biomass spectrum is defined as $B_s(m) = B_i / \log\left(\frac{m_i^+}{m_i^-}\right)$ (Andersen and Visser, 2023).

In the following, we describe the results of the first-level randomized parameter studies and the subsequent detailed studies. The shared aim of these investigations is to better understand NUM model behavior, performance relative to observations, and of how much parameter choice influences model results.

425 4.2 First-level random parameter study: can the model reproduce the planktonic community biomass structure?

We initially ~~test~~tested the model's ability to reproduce the biomass spectrum and the community size spectrum of the California Current Ecosystem (CCE). Just as important, this is also a test of the variability that parameter choices have on the model result. The result of the simulations is illustrated in Taylor diagrams (Fig. 4). The Taylor diagrams provide a visual representation of the normalized standard deviation (STD_m/STD_o ; radial distance from origin shown as grey solid line), correlation (COR_{m-o} ; azimuthal positions) and the centered root-mean-square difference ($cRMS_{m-o}$; black circles extending out from the grey dot) of the 100,000 model simulations, compared to the annual averaged observations from CCE (represented by the grey dot). The bright yellow color in the first quadrant of all five diagrams show that the model simulations generally ~~results~~result in a positive correlation coefficient with the CCE-LTER observations on all biomass size categories. The smallest effect of parameter variations is seen on the autotrophic microplankton ($B_{A-micro}$, Fig4e) where solutions are centered in a smaller area than the other four size categories. On the other end of the scale autotrophic picoplankton show the largest spread in solutions from randomizing the parameters (B_{A-pico} , Fig4c). On average, the smallest difference between model result and the mean observations (determined as $abs(1 - mean(cRMS))$) is found for B_{T-nano} which, despite some simulations with a negative correlation, generally show the closest fit to observation. The other four categories have a larger deviation from observations due to either lower pattern agreement (COR_{m-o}) or over- or underestimation of the amplitude of variations (STD_m/STD_o). The ~~pico- and nanoplanktonic size groups all overestimate the~~ amplitude of variation in the size spectrum is overestimated for all size groups of pico- and nanoplankton while the model underestimate the amplitude of variation in the autotrophic micro plankton. The pattern agreement is overall best for B_{T-pico} and B_{A-nano} with mean correlation of 0.87 and 0.80. Interestingly, the result of the simulations falls within three distinct groups for B_{A-pico} , where some parameter combinations produce a much better correlation with observations than ~~other~~others. That B_{A-pico} fall in three groups may be related to the biomass quantization also found in observations and other size-structured planktonic ecosystem models (Moscoso et al., 2022; Schartau et al., 2010).

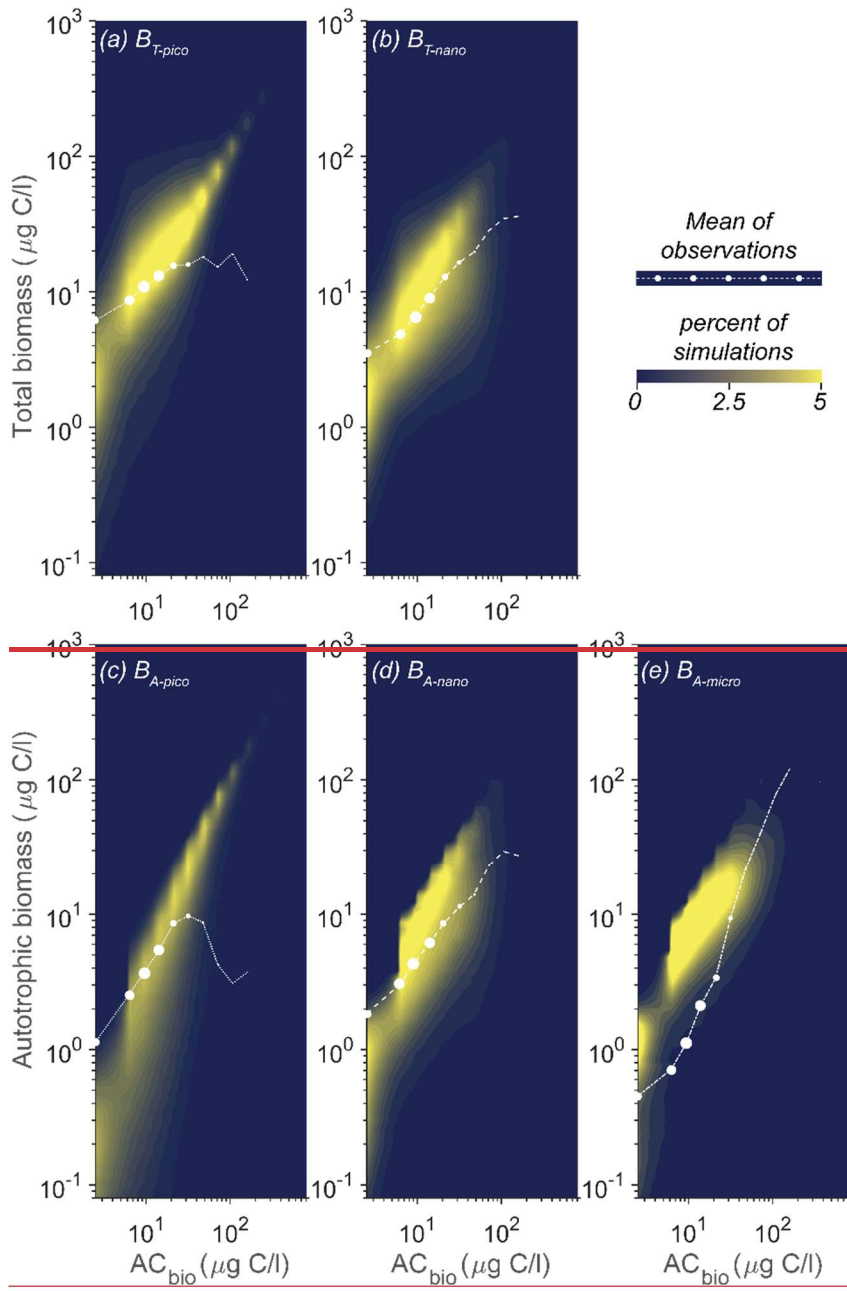


450 **Figure 4: Taylor diagrams for 100,000 random parameter combinations at CCE, displaying the standard deviation (STD) of the model result relative to observations (Obs.), and correlation coefficient (COR), and centered root-mean-square-difference (cRMS) between model and observations. Blue to yellow color reflect increasing number of realizations in each area. B_T and B_A ~~defined are~~ defined in figure 2.**

455 An alternative way to get an overview of the model's capabilities and parameter effect is ~~to do visualization~~ visualize of the overall trend in simulations compared to the observation data as a density plot (Fig. 5). The coloring on the figure show that most of the simulations for the five size categories have a power-law increase of the biomass with increasing AC-bins. Generally, ~~the model does not capture the occurrences of~~ there is a lack of model results with biomass concentrations into ~~the~~ high AC_{bio} concentrations bins (AC_{bio} above approximately $100 \mu\text{g C/l}$), which is consistent with the observation that only
 460 2% of the samples have autotrophic biomass concentrations of $100 \mu\text{g C/l}$ or above, here illustrated by the size of the white dots. The trend in simulations corresponds relatively well with observations for B_{T-nano} (compare to mean observations given

as white dots) which also showed to be the size category with the lowest cRMS (fig. 4). The trend in $B_{A\text{-nano}}$ simulations also aligns reasonably well with observations, though the correlation is slightly weaker due to a larger discrepancy between the modelled increase in biomass and the observed increase in biomass. Both size groups of nanoplankton do however
465 underestimate the biomass at low AC_{bio} -bin ($AC_{\text{bio}} < 10 \mu\text{gCl}^{-1}$) and overestimate the biomass at higher AC_{bio} , corresponding with the greater-than-observed amplitude of variations in the Taylor diagrams. The picoplanktonic size groups also exhibit a gradual increase in biomass with increasing AC_{bio} , rather than the plateau at intermediate-high AC_{bio} seen for observations of $B_{T\text{-pico}}$ and the decrease in biomass for $B_{A\text{-pico}}$. Additionally, the model underestimates biomass at low AC_{bio} for both picoplanktonic size groups. The modelled amplitude of variation for $B_{A\text{-micro}}$ is lower than the observations which manifest as
470 a too high biomass at low AC_{bio} and a lower-than-observed increase in biomass with increasing AC_{bio} .

475



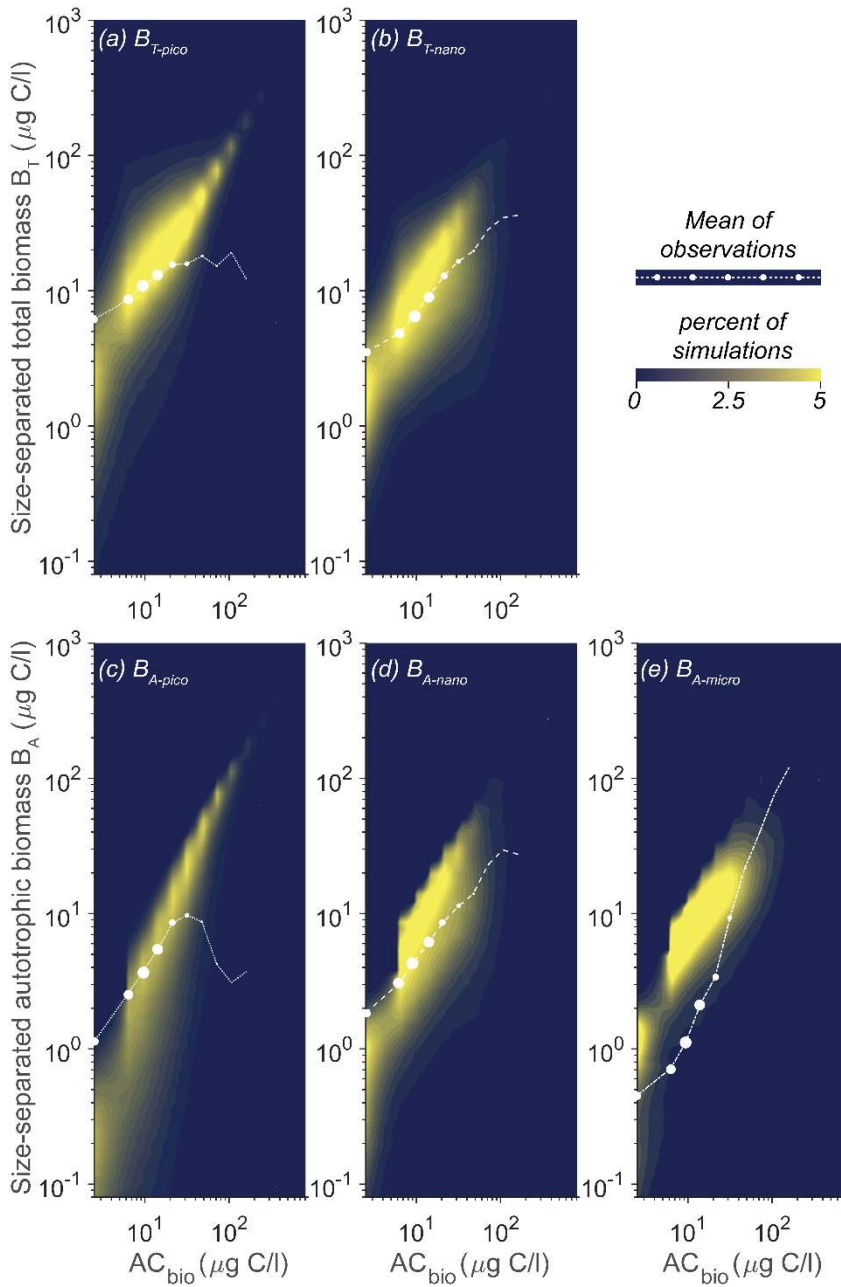
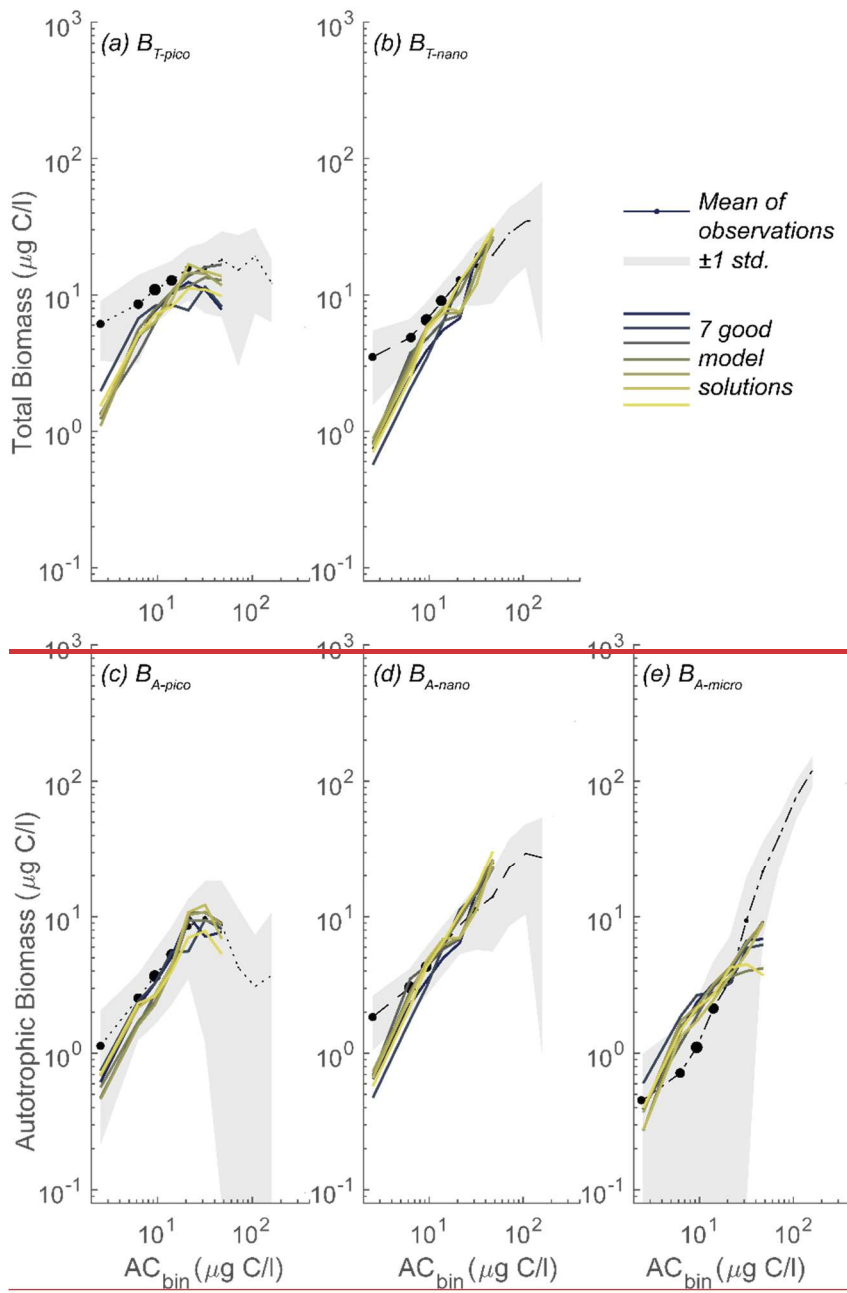
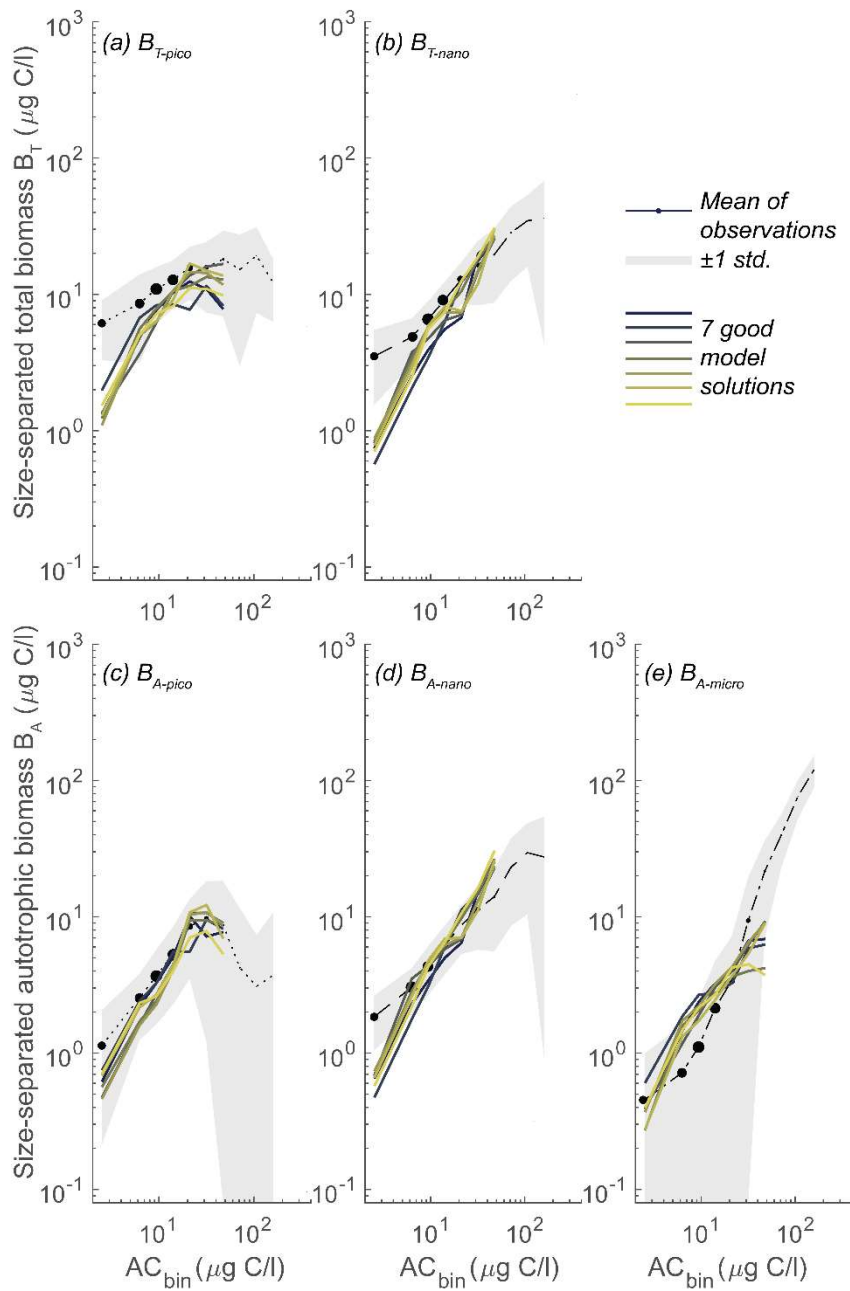


Figure 5: Model mean and total biomass of size groups as a function of total biomass for 100,000 random parameter combinations at CCE. White dots are observations in AC_{bio} bins. Abbreviations as figure 2. Blue to yellow reflect **increasing an increasing** number of realizations in each area. **Size**The size of white observations dots **indicate indicates** the relative number of observations in that AC_{bio} bin. Note the tendency of NUM to under-estimate pico- (a,c) and nanoplanktonic (b,d) biomass at low AC_{bio} while overestimating the biomass at intermediate-high AC_{bio} . The autotrophic microplanktonic biomass (e) is generally overestimated.

Of the completed model calculations, the ideal parameter combinations should result in $COR_{m-o} > COR_{iao}$ and $RMSd_{m-o} < RMSd_{iao}$ for all size groups. Evaluating these conditions ~~show~~shows that none of model results fulfill both criteria for all size groups. A detailed examination of the simulations in term of COR_{m-o} and $RMSd_{m-o}$, however, ~~reveal~~reveals a subset of seven simulations that result in a planktonic size variability that corresponds particularly well with the observations (Fig. 6).





490

Figure 6: Model mean and total biomass of size groups as a function of total biomass for the 7 statistically most optimal parameter combinations at CCE. Black dots are observations in AC_{bio} bins. Abbreviations as Fig. 2. Note the tendency for NUM to underestimate pico- and nanoautotrophic biomass at very low AC_{bio} and overestimate microautotrophic biomass.

495 In these seven simulations the picoplanktonic size groups align with the mean observations, showing a plateau at intermediate-high AC_{bio} for B_{T-pico} and a tendency for biomass to decrease for B_{A-pico} at AC_{bio} above $30 \mu gCl^{-1}$ (Fig. 6a, c). The parameter combinations do however result in B_{T-pico} lower than one standard deviation for the smallest AC_{bio} bin. Both nanoplanktonic size groups closely follow the observations, though still with lower-than-observed biomass at low AC_{bio} (Fig. 5b, d). The trend in microautotrophic biomass aligns with most of the model results, which generally show higher-than-
500 observed biomass. These results fall on the lower end of the 100,000 simulations but are still too high at low to intermediate autotrophic biomass levels (approximately 4-30 $\mu gC/L$), forming a “humped back” shape (Fig. 5e). While these seven simulations correlate remarkably well with the observations, the seven simulations general have slightly too low correlation coefficient for $B_{A-micro}$ (0.79-0.95 for model results versus 0.96 for observations) and too high root-mean-square-difference for B_{T-pico} (0.48-0.64 versus 0.4) and B_{T-nano} (0.37-0.71 versus 0.3) (the statistic is available in Supplement S3).

505 With the goal of identifying a parameter range that yields robust optimal solutions, we will focus on this subset of seven simulations that ~~perform~~perform especially well in the further sensitivity analyses of the parameters. We use the identified seven sets of parameters to define a *restricted parameter span* based on the on minimum and maximum of each parameter in the set group (Fig. 7, blue lines).

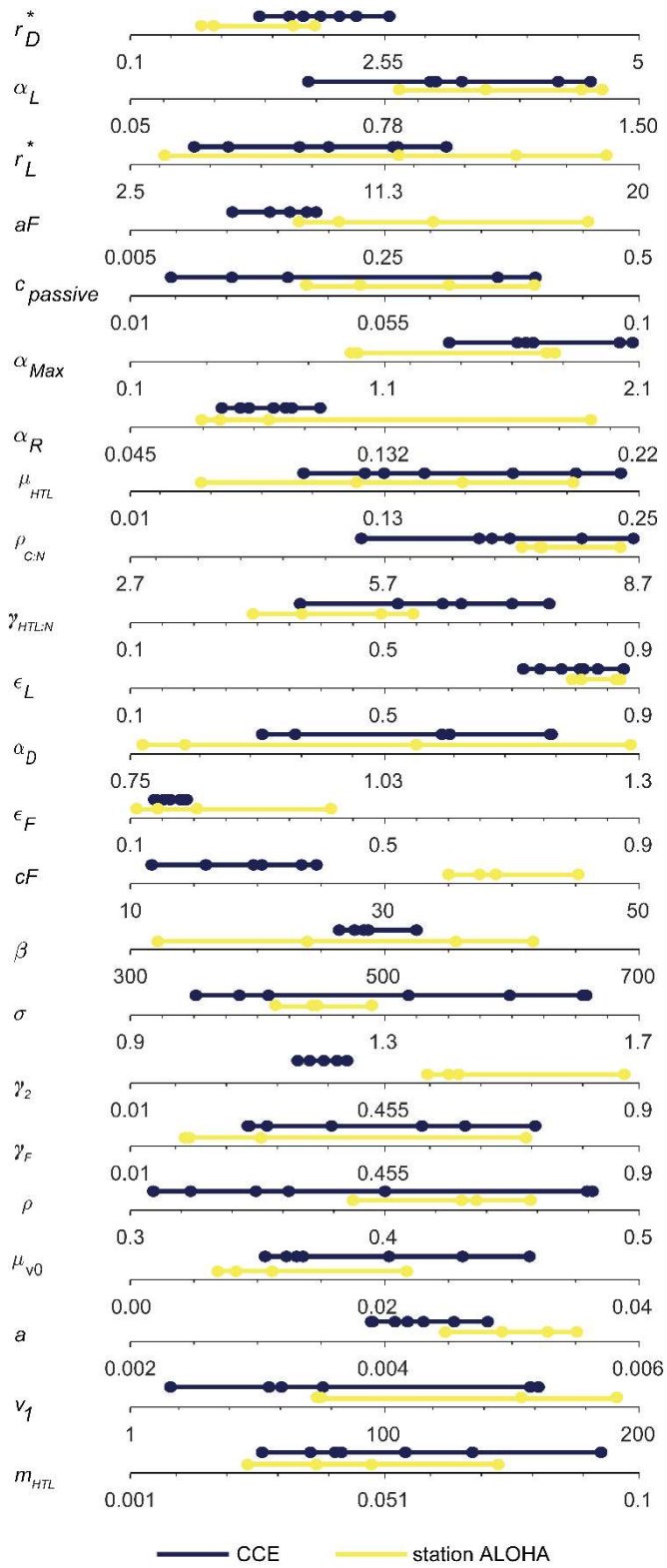


Figure 7: Span of all free model parameters for the seven most optimal parameter combinations at either CCE (blue) or Station ALOHA (yellow). The seven CCE model results are shown in Fig. 6. Note how the parameter spans for CCE and Station ALOHA generally follows the same trend except for γ_2 and cF where higher values are needed to fit the data at Station ALOHA than CCE. The most optimal parameter combination is estimated by highest correlation coefficient and lowest root-mean-square difference between model and observation simultaneously for B_{T-pico}, B_{T-nano}, B_{A-pico}, B_{A-nano}, and B_{A-micro}. Parameter definitions in Table 1 and other abbreviations in Fig. 2.

4.3 Restricted parameter span and sensitivity

We will now aim to evaluate the importance of the parameter uncertainties and to establish a stable parameter space for the 23 free parameters, wherein the simulations yield a reasonable result. The range of each free parameter is based on the range defined by the seven solutions with optimal fit (Fig. 6). An initial local parameter sensitivity assessment revealed a high degree of non-linearity in the model that makes it difficult to make any global conclusions about parameter influence based on local studies. To gain more insight into how the parameters influence the sensitivity of the entire non-linear ecosystem system we instead perform a global sensitivity analysis (Bilal, 2014; Sobol, 2001; Zhou and Lin, 2008).

Figure 8 displays the parameters ranked by Sobol's total sensitivity index (STi) based on root-mean-squared difference for the five size groups. The corresponding figure based on correlation is available in Supplement S6, but its conclusions are consistent with Fig. 8. The value of the index cannot be compared across the different categories but the span in values gives an indication of the variability in the sensitivity across parameters. For example, while B_{T-pico} seems to be especially sensitive to approximately half of the parameters there is little difference among the parameter sensitivity for B_{A-micro}. The global sensitivity analysis reveal that all size groups are sensitive to the choice in parameters that control mortality (red dots): phagotrophy (the phagotrophic assimilation rate (ϵ_F), clearance rate (aF), the predator-prey ratio (β) and width (σ), higher trophic level mortality (HTL pressure (μ_{HTL})), and viral lysis (μ_{v0}). All size groups are also sensitive to the value of maximum rate of biosynthesis (α_{max}) and to a smaller degree respiration (α_R) (grey dots). Parameters such as the remineralization rate of dead organisms (γ_2 , purple), diffusive affinity cross-over (r^*_D , except for B_{A-micro}, blue), and the C:N ratio of the cell are among the moderately sensitive parameters. The parameters mentioned above are parameters that control the predation pressure, biosynthesis and nutrient availability and uptake. Finally, the analysis shows that the picocautotrophic biomass is more sensitive to the light uptake efficiency (ϵ_L , yellow) parameter than the other size groups. The analysis shows that other parameters are less important and therefore allows for larger uncertainties. These parameters include the carbon density of the cell (ρ), passive losses coefficient ($c_{passive}$), and the remineralization of feeding losses (γ_F) and higher trophic levels (γ_{HTL}).

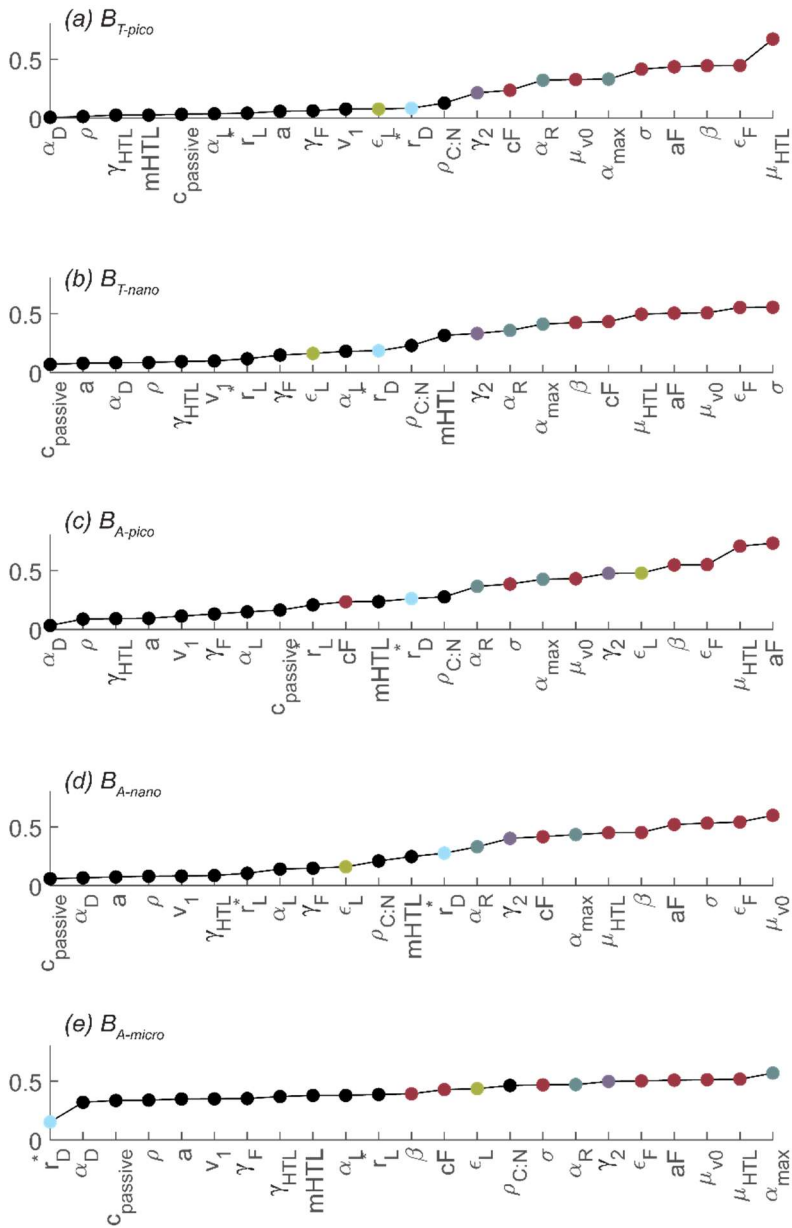
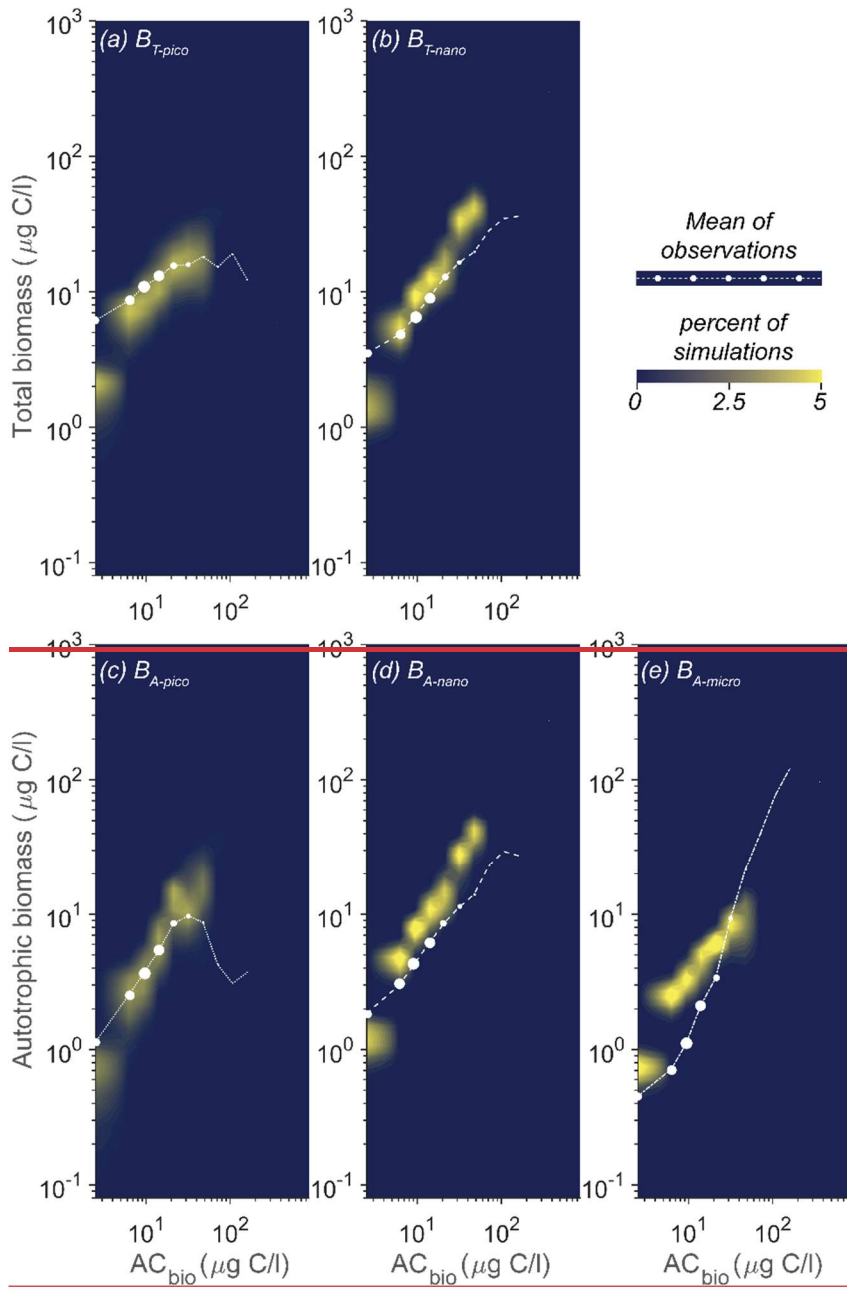


Figure 8: Global parameter sensitivity ranked based on sensitivity index calculated by Sobol's variance-based sensitivity method for non-linear models. Sensitivity calculated for RMSd. The parameters that the NUM model is most sensitive to have been colored according to categories: predation and mortality (red), synthesis (grey), cell remineralization (purple), light uptake efficiency (yellow), diffusive affinity cross-over (blue). Note how all biomass size are especially sensitive to parameters controlling predation (red dots), and synthesis (grey dots). Parameter definitions in Table 1 and other abbreviations in Fig. 2

545

While the model sensitivity towards parameters is complex and non-linear, a final set of 10,000 random parameter simulations demonstrate that the model result space can be reduced by confining the parameter space to the restricted parameter span found in Fig. 7. Using the restricted parameter span we see a tighter fit of model results to observations (Fig. 9) in contrast to the full randomized parameter spans (Fig. 5). The parameter restrictions have removed the simulations that produced excess pico- and nanosized biomass at high AC_{bio} and the simulations now follow the observed trend with an onset of a plateau at AC_{bio} of $20 \mu\text{gCl}^{-1}$ for B_{T-pico} and B_{A-pico} . The restriction has had less impact on the nanoplanktonic biomass but has narrowed the range of results, leading to a slight overestimation of nanoplanktonic biomass in most simulations, particularly at AC_{bio} levels above $30 \mu\text{gCl}^{-1}$. Overall, the model results in Fig. 9 demonstrate a notable improvement in model performance for the identified parameter spans in comparison to the full parameter space. While this improvement may seem intuitive it is not necessarily a priori given, considering the model's parameters non-linear response to parameter change. The local sensitivity analysis showed that, even within the restricted parameter space, the impact of varying a parameter is highly dependent on the other parameters (Fig. S2). The restricted parameter space could therefore, in theory, have resulted in the same degree of model misfits as the full parameter span with only a few acceptable solutions generated by very specific parameter combinations. That the model performance is enhanced by restricting the parameter span This suggests that further detailed parameter tuning may not be necessary to achieve reliable results from the NUM model. While a better performance ~~this~~ is encouraging it is important to evaluate if the identified parameter spans are applicable to other biogeographic provinces.



570

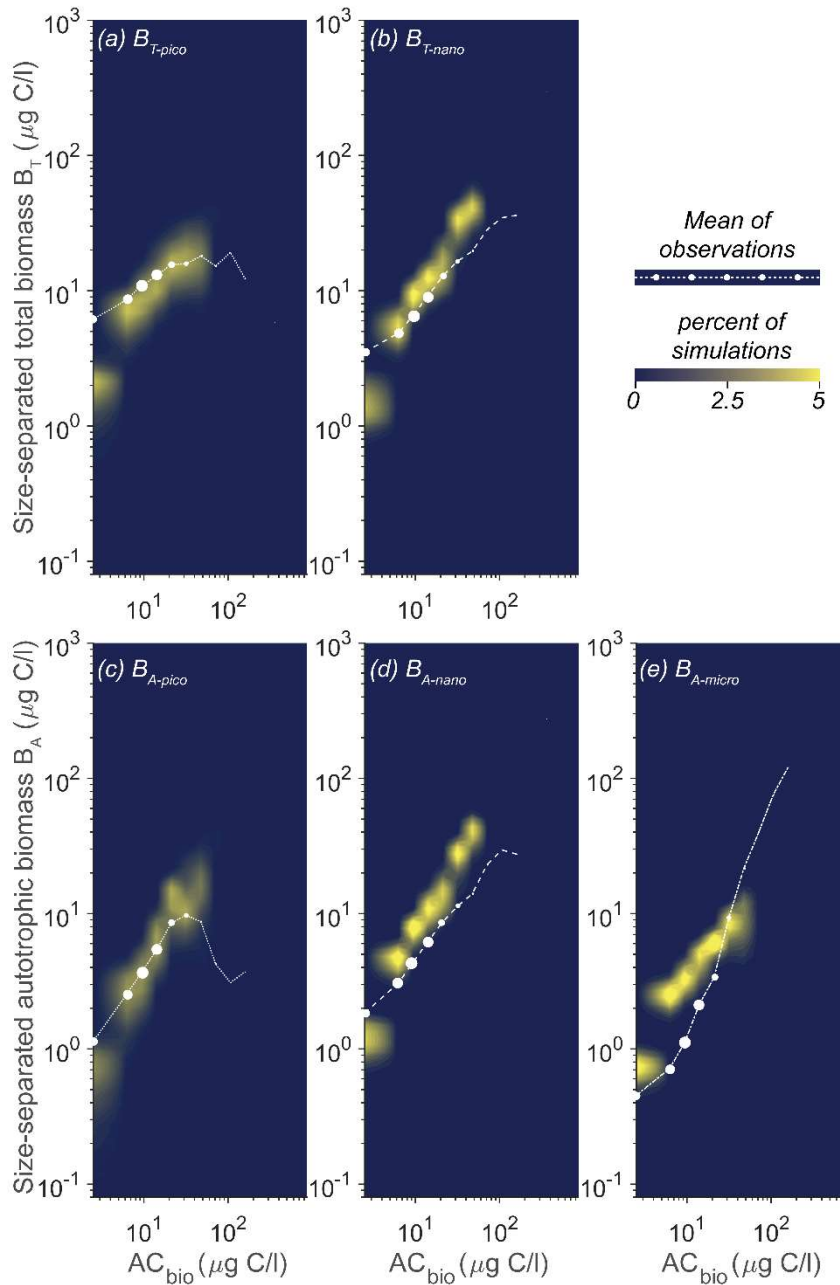
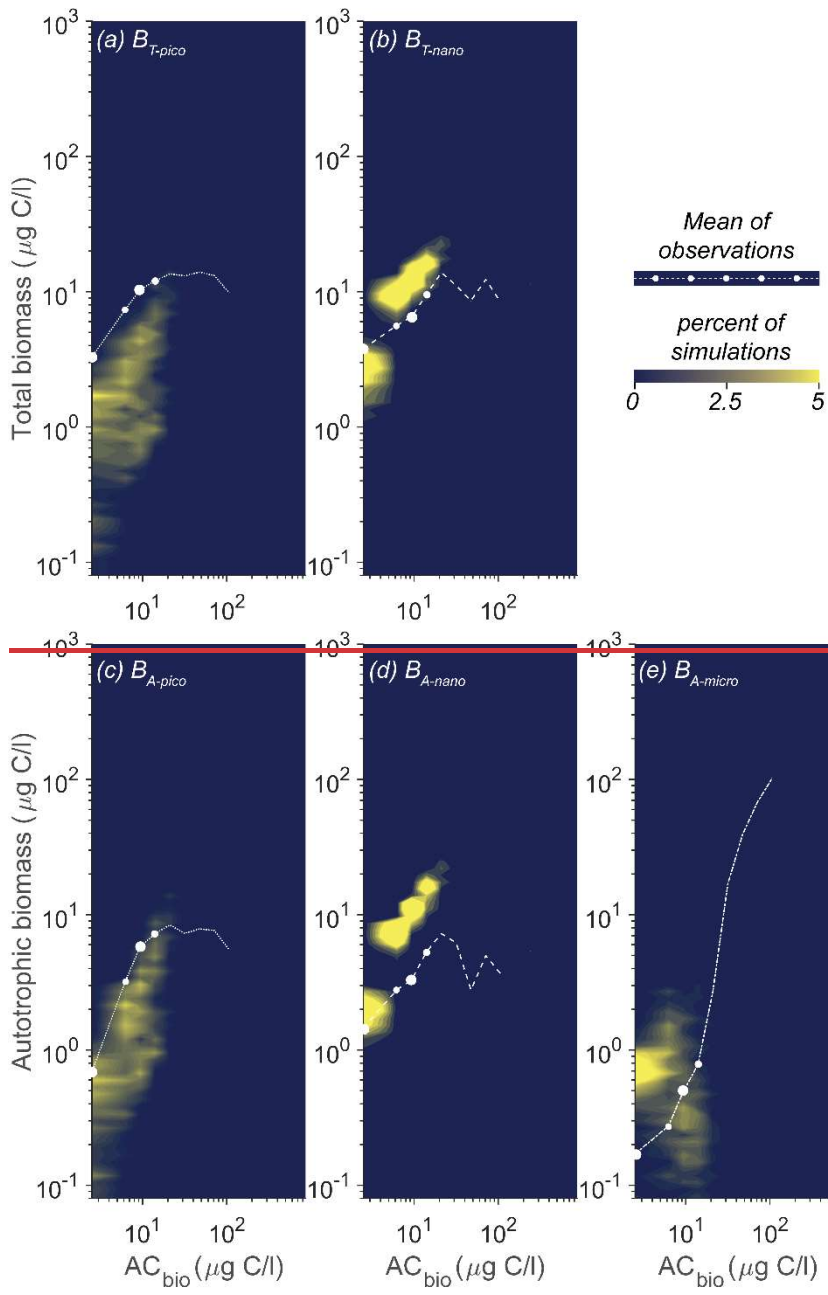


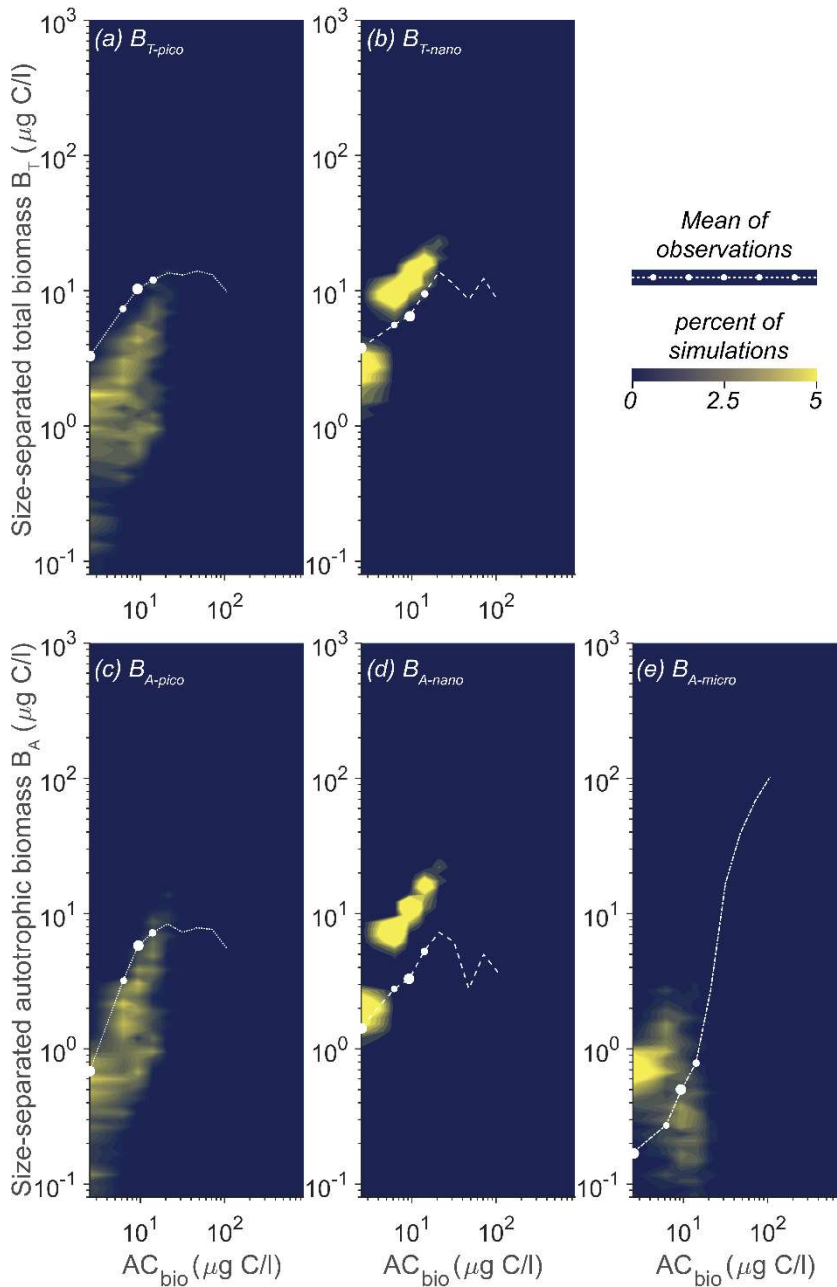
Figure 9: Model mean and total biomass of size groups as a function of total biomass for 10,000 random parameter combinations sampled within the restricted span of parameters at CCE. The random parameter spans are based on the parameter range of the seven statistically optimal parameter combinations at CCE (see text). White dots are observations in AC_{bio} bins. Abbreviations as Fig. 2. Blue to yellow reflect increasing an increasing number of realizations in each area. Note how the solution space has been restricted, especially for picoplankton (a,c) compared to the full parameter span (Fig. 5).

575

4.4 Results for Station ALOHA

The heart of the trait-based approach is its potential universality; the principle that a single set of parameters can describe organisms and ecosystems across time and place. An important test is therefore if the parameter sets that performed best at CCE are suited for different oceanographic settings. Figure 10 ~~show~~shows the result of 10,000 simulations with conditions mimicking Station ALOHA with quasi-random parameters from within the restricted parameter span defined for CCE. The model reacts to the shift in oceanographic regime by lowering the overall autotrophic biomass. Most simulations only reach a biomass of $20 \mu\text{g C l}^{-1}$ which is consistent with observations. The biomass of the picoplanktonic size groups is lower than mean observation but generally within one standard deviation (Fig 10 a, c and see Fig. 2b for comparison). Both nanoplanktonic size groups exhibit elevated biomass relative to observations, with the discrepancy being larger than that observed for the nanoplanktonic size groups in the CCE simulations (Fig 10b, c, compare with Fig 9b, c). The microautotrophic size group exhibits the poorest correlation with mean observations, displaying excessive biomass at low AC_{bin} ($< 9 \mu\text{g C l}^{-1}$) and variable, but lower biomass at AC_{bin} above $9 \mu\text{g C l}^{-1}$. This pattern is inconsistent with the observed sigmoidal trend, although the biomass falls within the standard deviation of the observations (Fig 10e, compare with Fig. 2b). A comparison to the first-level random parameter simulation with 100,000 simulations within the full parameter space (not illustrated here but available in Supplement S7) show that restricting the parameters based on the solutions from CCE has removed a set of simulations that produced too large biomasses for all size categories at intermediate AC-bins. However, it also eliminates a set of simulations with better fitting biomass concentrations at low AC_{bio} -bins. Figure 11 ~~show~~shows a set of simulations from the first-level random parameter study that performs particularly well for Station ALOHA. In these simulations, both pico- and nanoplankton follow the trend of the observations and exhibit the correct amount of biomass. Interestingly, most of the parameters for these four simulations fully overlap with parameter for the best solutions at CCE (Fig. 7). While some parameters such as a_F and α_{max} only partly overlap, the only parameters only significantly differ that significantly differ between the two sites are from the parameter for the best solutions at CCE by having higher γ_2 , c_F that both have higher value at Station ALOHA than CCE. -and partly a_F values (Fig. 7). The parameter γ_2 controls the fraction of dead matter directly remineralizer back to nutrients and it areis thereby an important parameter in controlling the amount of osmotrophy for the smallest planktonic size group. c_F and a_F are two important components of the rate of phagotrophy. It is noteworthy that the parameters for successful solutions at the two different sites exhibit parameter trends in many cases correlate; for both stations, the successful simulations have relatively high α_L , α_{max} , $\rho_{\text{C:N}}$, ϵ_L , a ; a , and low ϵ_F .

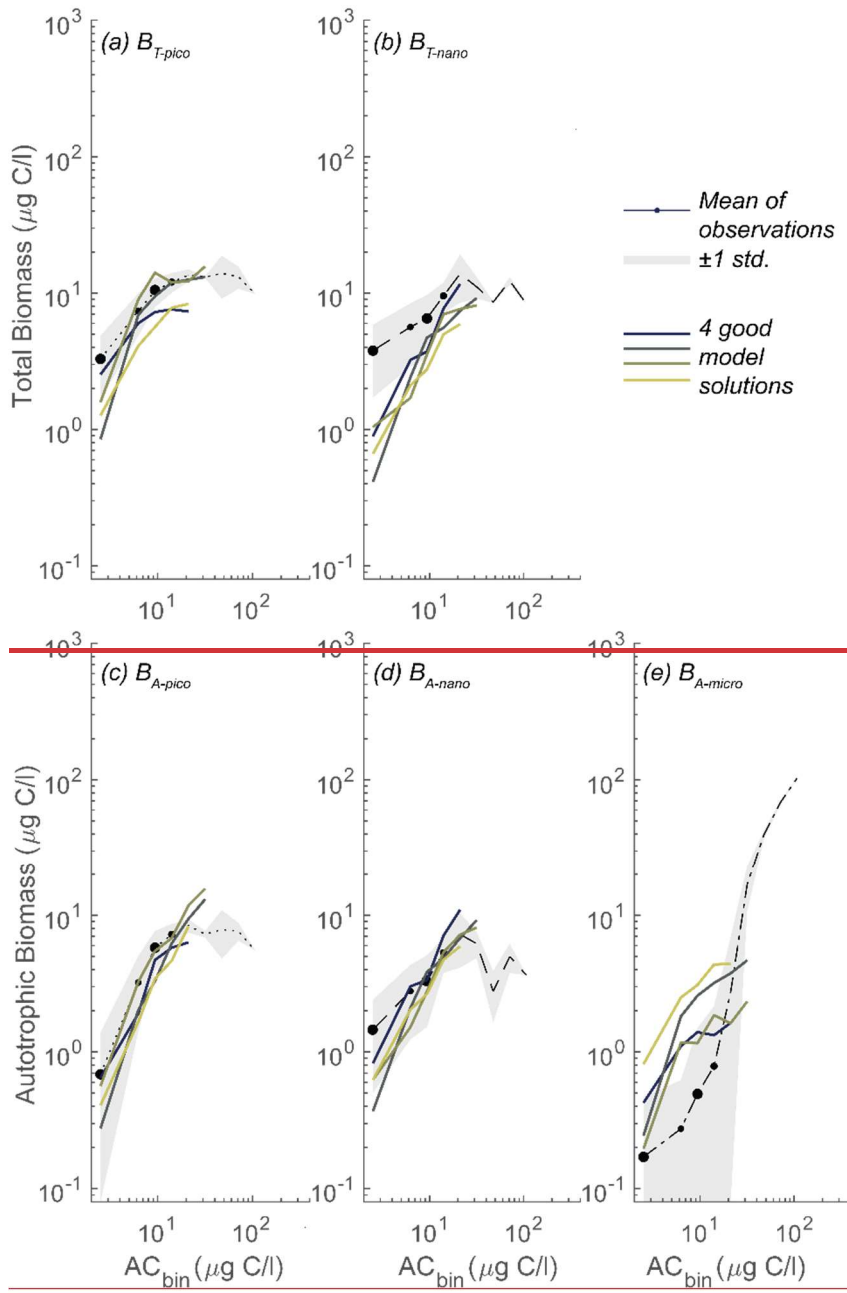




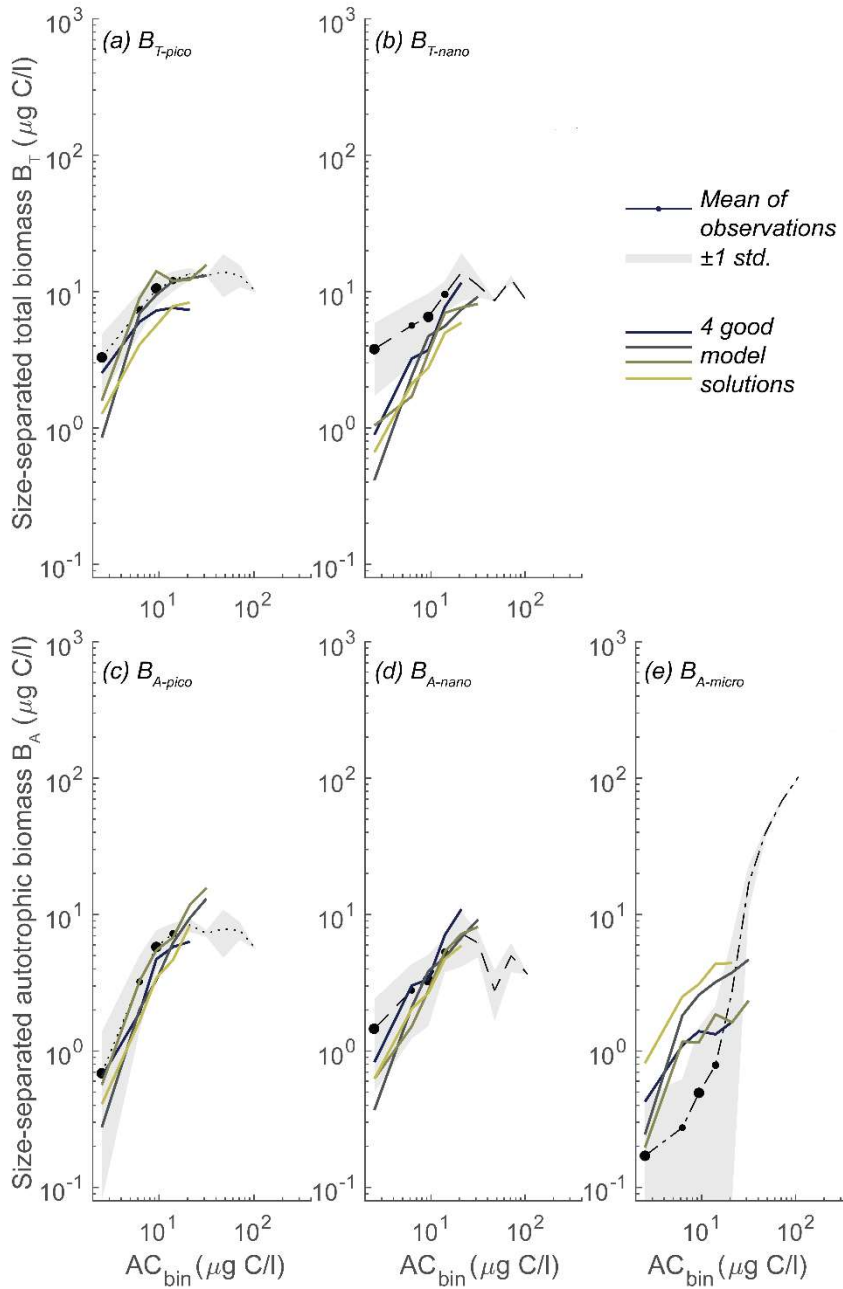
610

Figure 10: Model mean and total biomass of size groups as a function of total biomass for 10,000 random parameter combinations at Station ALOHA. The simulations have random parameter combinations within the restricted parameter space based on the successful simulations from CCE (Fig. 7). White dots are observations in AC_{bio} bins. Abbreviations as Fig. 2. Blue to yellow color reflect increasing number of realizations in a given area. Note how biomass of pico plankton (a,c) is underestimated while nano

615 plankton (b, d) is generally overestimated. Microautotrophic plankton (e) has the lowest correlation of the five size classes with decreasing biomass as a function of AC_{bio} .



620



625 **Figure 11: Model mean and total biomass of size groups as a function of total biomass for the four statistically most optimal parameter combinations at Station ALOHA. Black dots are observations in AC_{bio} bins. Abbreviations as Fig. 2.**

4.5 Nutrient profiles

As an indirect way of evaluating the model performance and response to the different environmental conditions, we also evaluate the depth profile of model nutrients for the two sites (Fig. 12). Importantly, the nutrient profile was not part of the initial statistical measures used to identify the model parameters. The nutrient profiles for CCE are remarkably consistent across the solutions. Nutrient concentrations are low in the upper photic zone and increase with depth. While the modelled profiles generally align with the observed data, there is a tendency to underestimate nitrate concentrations at depths ranging between 50 and 200 meters. For Station ALOHA, the modelled profiles also align well with the measured concentrations, with a slight tendency to overestimate nutrient concentrations at depth. The model is generally able to respond correctly to the shift from eutrophic to oligotrophic conditions.

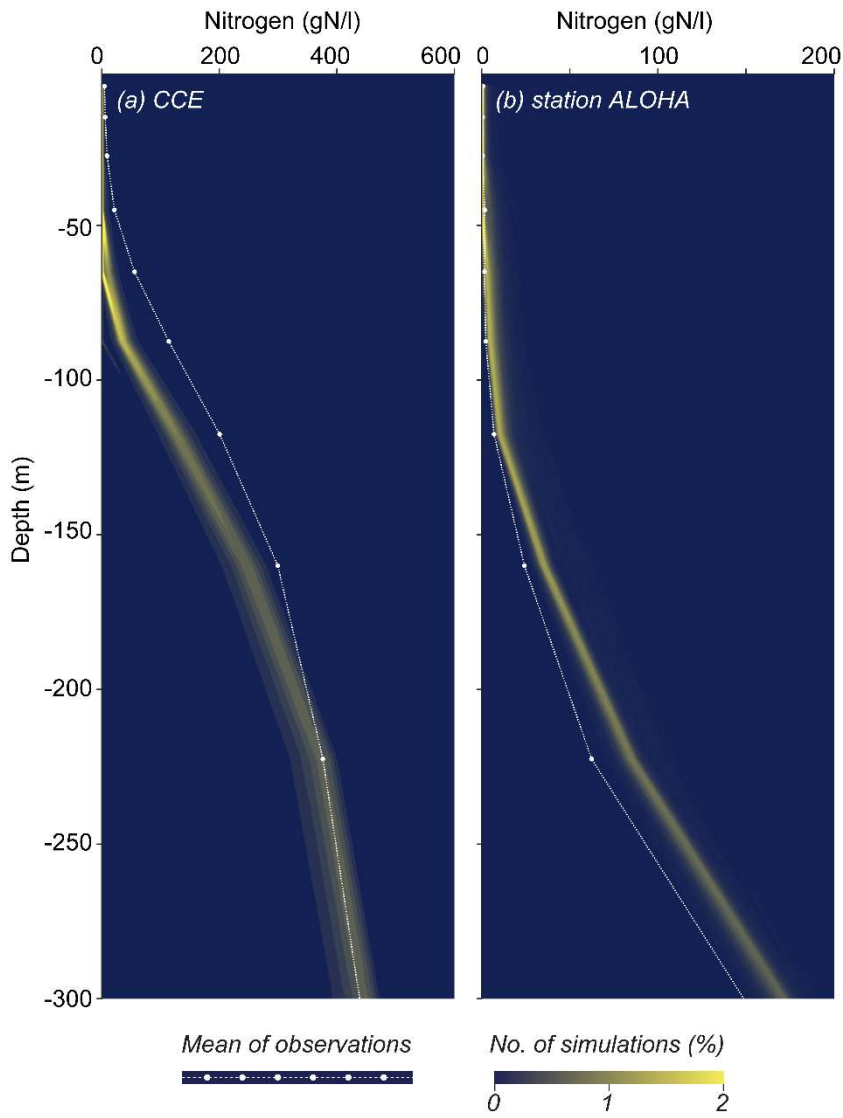


Figure 12: Model nutrient profiles at CCE (a) and Station ALOHA (b). White dots are observations based on (Calcofi-Scripps-Institution-of-Oceanography and Wilkinson, 2022; Pasulka et al., 2013; Garcia, 2018). Note the model tendency to underestimate N in the thermocline at CCE, but overestimate at Station ALOHA.

640 5 Discussion and Perspectives

5.1 Summary of model performance

We have validated the generalist unicellular NUM ecosystem model toward two quite different biogeographic provinces: the high productivity upwelling conditions of the California Current Ecosystem and the oligotrophic downwelling conditions

at Station ALOHA. For the California Current Ecosystem, out of 100,000 random combinations of the 23 free parameters a large majority of the model results have correlation coefficient toward observations (COR_{m-o}) better than 0.7. This demonstrated that the generalist unicellular NUM model, despite its simplicity, ~~is able to~~ capture the size distribution of the planktonic ecosystem and its nutrient profile over a broad range of parameter values. Out of the random simulations we find only seven optimal, but quite different, parameter combinations that reproduce results for the CCE. These seven optimal simulations almost perfectly match the distribution of each of the size groups as ~~function~~ of increasing AC_{bio} (Fig. 6). The seven optimal parameter combination have mean COR_{m-o} of 0.94 and $RMSd_{m-o}$ 0.4 for the five size groups considered in comparison with observations. In particular, we find that B_{A-pico} peak and B_{T-pico} plateau at intermediate levels of autotrophic biomass in agreement with observations (Taylor and Landry, 2018) (Fig. 6a,c). We also find a power-law increase in B_{T-nano} and B_{A-nano} as function of AC_{bio} as in observations (Fig. 6b, d). Finally, we observe a "humped back" increase in $B_{A-micro}$ that has the lowest correlation to observations but still within one standard deviation of the observed total mean (Fig. 6e).

Moving to oligotrophic ALOHA station, we find that the seven optimal model parameter combinations from CEE give model results that capture many important aspects of the observational data. NUM qualitatively model a reduction in biomass at Station ALOHA relative to CEE and it generally reproduce the overall size structure. That the NUM model produces less biomass at ALOHA is consistent with observational differences between CEE and ALOHA (Taylor and Landry, 2018). The seven simulations do however produce too low picoplanktonic biomasses and too high nanoplankton biomasses, compared to the observations. A detailed analysis ~~shows~~ that another set of parameter combinations were better at reproducing the pico- and nanoplanktonic biomass both in term of correlation and overall biomass values. The parameter space for these simulations were only significantly different from the restricted parameter span for CCE in their range of a few parameters (discussed below). Our validation against ALOHA overall indicates that by restricting the parameters ~~to a restricted span~~, based on the seven optimal models at CCE, and focusing on this small set of parameters, it is possible to match the overall increase and decrease in biomass for the different size classes to a degree that would be satisfactory for applications where site-by-site calibration is not possible.

5.2 Parameter sensitivity

Our sensitivity analysis shows that the model parameter sensitivity is dependent on the specific parameter combinations and that the ecosystem response is non-linear. Local sensitivity analysis revealed that while one of the good solutions was nearly equally sensitive to almost all parameters, another was mainly sensitive to only one parameter (ϵF , Fig S2 in Supplement 4). ~~Based on~~ Through a global sensitivity ~~analysis~~, we ~~isolated which~~ identified the parameters that are especially controlling (Fig. 8). Parameters regulating predation ~~and mortality~~, biosynthesis, and respiration are generally important among all size groups. Changes in these parameters create the largest shifts in the model output. ~~Interestingly,~~ many of the parameters that produce the largest shifts in biomass are also among the least constrained (Table 1; cf. (Andersen and Visser, 2023)). In the following discussion we focus on the parameters that are the least constrained while

also resulting in the largest sensitivity. Higher trophic level mortality (μ_{htl}) is important for all size groups. μ_{htl} is an extrinsic parameter that governs predation rates by higher trophic levels. This parameter serves as a closure term in the model and plays a critical role in shaping biomass distribution. Specifically, μ_{htl} determines the size and biomass of microplankton, initiating cascading effects on smaller size classes. While μ_{htl} significantly impacts biomass partitioning across size groups, its influence on total biomass is limited because reductions in microplankton results in corresponding increases in nanoplankton (see Fig. 15b in Andersen and Visser (2023)). The value of μ_{htl} depends on the biomass and efficiency of higher trophic levels, which can vary significantly between eutrophic and oligotrophic environments. Our results indicate that optimal μ_{htl} is larger at CCE compared to Station ALOHA, although there is a significant overlap (Fig. 7). The importance of μ_{htl} suggests that including higher trophic levels, such as copepods, could reduce model uncertainties. However, that only shifts the problem towards determining the higher trophic level mortality on copepods, which is equally uncertain. Another highly uncertain parameter that creates large shift in the biomass distribution is the viral lysis mortality coefficient Andersen and Visser (2023) μ_{v0} . This parameter introduces a density dependent control of the population in each size group. It has the effect of increasing the mortality on groups with high biomass and prevents all biomass ending up in one or a few size groups. The principle of abundance controlled viral lysis is an important aspect of the “Killing the Winner” principle (Thingstad, 2000; Winter et al., 2010). The default parameter used in the NUM model is adjusted such that the effect of viral lysis is smaller than other mortalities, to avoid that this process is determining the result, despite that the value of the parameter is largely unknown. Based on the global sensitivity study it is an important future priority to get a better mechanistic understanding of the viral lysis mortality process. Two other important parameters, cF and ϵF are both involved in heterotrophic phagotrophy, and are partly multiplicative so one is influencing the other (cf. Eq. 3 Table 2). While the assimilation efficiency (ϵF) is relatively well-constrained the maximum phagotrophic coefficient (cF) is not. The parameter cF is unique to the NUM model and determines the phagotrophic assimilation limit for large cells. While cF only directly influences the largest cells it causes a cascading effect down the size spectrum. The default value used here is fitted against maximum growth rate for different types of plankton (see Fig. 5 in Andersen and Visser (2023)). Interestingly, cF is one of the only parameters that show significantly different optimal values for CCE and Station ALOHA (11-25 $\mu\text{g d}^{-1}$ for CCE versus 35-45 $\mu\text{g d}^{-1}$ for Station ALOHA). The difference is likely related to a tradeoff between food acquisition and predation, an important aspect of the slow-fast tradeoff (Salguero-Gómez et al., 2016; Kiørboe and Thomas, 2020). High rates of predation induces higher food acquisition but comes with a higher predation risk (Kiørboe and Thomas, 2020). The difference between CCE and Station ALOHA can therefore be seen as a difference between a more stable environment with high population densities (CCE) and varied conditions with strong environmental gradients (Station ALOHA). The same argument is valid for the phagotrophic clearance rate (aF), where the good fit for Station ALOHA has higher values compared to CCE. The mechanistic argument for phagotrophic clearance rate relates to the fluid dynamics of a beating flagellate cell (Nielsen and Kiørboe, 2021; Andersen and Visser, 2023). This mechanistic underpinning means that the value of aF is relatively well known, however with a scatter of one of magnitude due to difference in flagella arrangements that

710 generates difference in predation risk. Future investigations into patterns of flagella arrangements in different nutrient environments can maybe give some valuable insight into the trade-off between foraging and predation risk.

The last highly unknown parameter that can create large shifts in the biomass is γ_2 , that determines how large a fraction of the background mortality is remineralized directly into N and DOC instead of becoming POM. Increasing γ_2 increases the amount of dissolved nutrients and carbon in the system which increases the osmotrophic efficiency for picoplankton.

715 However, this value of γ_2 is highly uncertain, and cell mortality is treated quite simply here because of limited mechanistic understanding (Andersen and Visser, 2023). Apart from cF, γ_2 is the only other parameter where values are significantly different between the two sites. Values for γ_2 are larger at Station ALOHA than at CCE, indicating that a faster remineralization of organic matter is required at Station ALOHA. It is clear from the global sensitivity study that developing a clear mechanistic understanding of the fate of cell mortality should be an important priority. Fortunately, a mechanistic

720 model for organic matter accumulation has recently been developed which may be a way to improve the NUM model accuracy in future versions (Zakem et al., 2021).

Apart from the parameters described above, the model includes better established parameters that result in a relatively large sensitivity while also influencing the entire size spectrum. Of these, σ, β defines the shape of the prey-predator size distribution, and α_{max}, α_R controls the biosynthesis. In contrast, the effect of ϵ_L (light uptake efficiency) mainly influences picoplankton's affinity for photosynthesis. In contrast, the effect of ϵ_L (light uptake efficiency) mainly influences picoplankton's affinity for photosynthesis. Andersen and Visser (2023)The analysis shows that the parameter space for successful simulations overlap significantly between the two sites. The only parameters that are significantly different in the optimal parameter setup for the two sites are γ_2 , the parameter that determines how large a fraction of the background mortality is transferred directly into N and DOC, and the parameter cF that is involved in the calculation of phagotrophy.

725 Increasing γ_2 , increases the amount of nutrients and carbon in the system which increases the efficiency osmotrophic efficiency for picoplankton.

730 Increasing γ_2 , increases the amount of nutrients and carbon in the system which increases the efficiency osmotrophic efficiency for picoplankton.

Despite the model sensitivity to parameter changes, non-linearity and system bifurcation, the model appears to be relatively stable within the optimized restricted parameter spans identified based on comparison with CEE observations. Within the restricted se-spans, no parameter combinations seem to perform significantly better than others for the chosen metrics. We

735 recognize however that further local parameter sensitivity investigation can be useful with the current knowledge about the most important parameters gained from the global sensitivity study.

An underlying premise in our validation is that we compared the model results of a water column setup with annual-mean observations averaged-overaveraging nearly 700 km by 400 km including shelf and open ocean. This means that any parameter combination that performs well compared to the mean dataset will surely be less than optimal at some of the

740 individual stations or at specific times of the year. It would be interesting to Ongoing work is evaluatinge the NUM model in a regional ocean model where smaller variations along shelf and especially across the shelf can be resolved, and in settings were data permits resolution of seasonal variability.

5.3 Areas of improvement

We note that the optimal parameters spans have been determined with a water column model without vertical advection. CEE is particularly influenced by upwelling advection while Station ALOHA is influenced by convergence and downwelling advection. This difference is likely a significant factor contributing to the model deficiencies at ALOHA. Indeed the 100,000 random simulations at CEE tend to produce too low nitrate concentrations between 50 m and 200 m depth. This ~~indicating~~indicates that the model is missing additional upwelling that could push the nutricline up. It may be reasoned, that if there had been more physical upwelling in the model, the higher nutrient loading and presumably growth would mean that a new set of optimal parameter combinations would need to result in less biomass production to fit the observed biomass. The implication of more efficient biomass downregulation by perhaps more export would mean that for ALOHA, there would be more export driving the system more oligotrophic further enhancing the picoplanktonic biomass and lessen nano and microplankton. In fact, we see in the nutrient profiles that ALOHA has ~~a too~~high nutrient levels from 100 m and deeper. More downwelling advection in the model setup for ALOHA would push the nutricline down and result in a more oligotrophic system, perhaps shifting the ecosystem toward more picoplankton. Regardless, future investigating including a full two-way cross validation should explore NUM in a 3D circulation mode to alleviate model physics deficiencies of the current water column setup.

In the NUM model, there is only one generalist functional group where small to large are defined by the same parameter combination. This means that the smallest sizes, that are essentially bacteria in size, are modeled with the same set of parameters as larger eukaryotic phototrophs. It is well known that there is a myriad of different species of bacteria optimized with different metabolic strategies, optimized with different cell membranes, and with no mitochondria. For example, while the Prokaryotes *Synechococcus* and *Prochlorococcus* are of similar size the former inhabit the surface waters at Station ALOHA while the latter live at low light conditions near the nutricline (Wu et al., 2022). Further, while having quite different modes of life, their resource uptake and growth is also significantly different from for example pico- or nano-eukaryotes. In fact, large meta data analyses show very different allometric scaling of metabolic rate as function of body mass (size) (DeLong et al., 2010). Prokaryotes show superlinear scaling with a power of 1.7, while eukaryote protists have linear scaling with a power of 1. Thus, empirical observation seem to suggest that the parameters regulating biosynthesis in NUM may need to respond more strongly to size in the picoplankton end of the spectrum (cf. DeLong et al., 2010). In fact, our global sensitivity study revealed that the parameter regulating biosynthesis (α_{\max}) ~~are~~is among the most important parameters (Fig. 8). We furthermore found that the model in general could not capture picoplankton biomass in the oligotrophic system. ~~h~~However, the best fit between model and observations is with low r^*_D which increases the efficiency of the picoplanktonic community. If biosynthesis in the picoplankton range is modeled as more efficient than in for larger sizes, it potential would upregulate the microbial loop and result in more picoplankton biomass.

Another aspect related to too little pico-biomass under oligotrophic conditions may be related to the model treatment of DOM. Currently the model use DOC contributing only to osmotrophic heterotrophy. However, labile DOM has a

DOC:DON ~5-15 (Zakem and Levine, 2019). This means that under oligotrophic conditions the model osmotrophic bacteria are potentially nutrient limited missing an important source of nutrients that could boost the pico-microbial loop thereby increasing B_{T-pico} . Adding an explicit or implicit treatment of labile DON would likely result in better performance (cf. Zakem and Levine, 2019). Other recent studies have shown that the picoplankton *Prochlorococcus*, while predominantly
780 phototrophic, is capable of osmotrophic mixotrophy at low light conditions, and that labile DOM additions under low light boots the growth significantly (Wu et al., 2022). The experiments reveal that significant *Prochlorococcus* growth and biomass in the deep chlorophyll maximum is likely sustained by both light and DOM. Such additive substrate would increase the model picoplankton growth rate and boost B_{A-pico} to better match observations.

The simplicity of the NUM model puts some limitations on its use in some environments. The model does not yet include
785 oxygen nor reduction-oxidation reactions as in some trait-based models (cf. Zakem et al., 2020b; Zakem et al., 2020a). This has implications for the large phagotrophs or higher trophic level that are therefore not restricted in their respiration if for example oxygen is low. Using the model below the photic zone in upwelling systems and for investigating low-oxygen environments would require implementation of oxygen, a development that is underway. The model ecosystem is currently not limited by other nutrients than nitrate such as iron or phosphate (cf. Serra-Pompei et al., 2022; Serra-Pompei et al.,
790 2020). It might also be possible to capture more details of the ecosystem by parameterizing or adding additional functional groups such as diatom and bacteria, but these refinements come with a computational cost. Overall, the NUM model is fast and has the benefit of being able to resolve mixotrophy in organisms and shared predation, aspects attracting increasing attention in trait modelling (Wu et al., 2022; Casey et al., 2022; Follett et al., 2022). Our analysis shows that the model – overall and despite its simplicity – is remarkably stable within a wide range of parameters, and usable for a user without
795 intimate knowledge of the parameter settings.

6 Conclusion

We have validated the generalist unicellular component of the NUM ecosystem model framework in a water column setup for two sites - a high productivity upwelling system and an oligotrophic downwelling system. With optimization of the range of 23 free parameters, the unicellular component of NUM, despite its simplicity, ~~is able to can~~ capture the size distribution of
800 the planktonic ecosystem and its nutrient profile over a broad range of parameter values. The model reasonably reproduces the nutrient profile despite its simple POM and degradation formulation. For the California Current system (CCE) we find seven optimal ~~parameterparameters combinationcombinations~~ that are quite different but almost perfectly match the distribution of each of the size groups as function of increasing AC_{bio} . Validation against ALOHA overall indicate that by
restricting the parameters based on the optimal parameters for CCE and increasing the microbial loop (increasing γ_2) and
805 focusing on predation, there is a reasonable match to the overall trends in biomass for the different size classes and the nutrient profile. We find there is a tendency for NUM to underestimate pico- and nanoplankton biomass at both sites,

indicating that osmotrophy, nutrient uptake and/or mixotrophy in the lower range of the picoplankton group require further development.

810 Despite its simplicity, the NUM framework is remarkably stable within the identified restricted parameter ranges and likely well suited for modeling poorly known regions and evolutionary scenarios where first-principles trumps details.

7 Code availability

The NUM model used in this analysis along with scripts for running experiments, analyzing results and data, and plotting figures is available at https://github.com/trinefrisbaek/NUM_0.91_ModelEvaluation (815 <https://zenodo.org/doi/10.5281/zenodo.10844336>). The readme file contains a list of relevant scripts for running and plotting files. The original NUM code analyzed in this paper is available at <https://github.com/Kenhasteandersen/NUMmodel/releases/tag/v0.91>. The simulations are done with the MITgcm_2.8deg transport matrix that has to be downloaded separately from <http://kelvin.earth.ox.ac.uk/spk/Research/TMM/TransportMatrixConfigs/>.

820

8 Author contributions

TFH ran the simulations, edited the original NUM model, performed the analysis, and created the figures. CJB and TFH conceptualized the study and ~~curated~~processed the observational datasets. TFH prepared the manuscript with contributions from all co-authors. All authors participated in discussions and provided valuable ideas.

825 9 Competing ~~interest~~interests

The authors declare that they have no conflict of interest.

10 Acknowledgement

We thank Michael R. Landry for sharing his data from Station Aloha and his insight into the sampling method, as well as James Wilkinson and the team behind the measurement from the CalCOFI cruises. This work was supported by Villum Fonden Grant 16518, by VKR Center for Excellence “Ocean Life”, ~~and~~ Independent Research Fund Denmark (10.46540/2032-00265B), ~~and~~ Simon’s Foundation grant 931976. ~~CC~~JB secured computation resources on the PALEOK cluster and Computerome 2.0 clusters, at University of Copenhagen.

References

- 835 Andersen, K. H. and Visser, A. W.: From cell size and first principles to structure and function of unicellular plankton communities, *Progress in Oceanography*, 213, 102995, <https://doi.org/10.1016/j.pocean.2023.102995>, 2023.
- Andersen, K. H., Aksnes, D. L., Berge, T., Fiksen, O., and Visser, A.: Modelling emergent trophic strategies in plankton, *Journal of Plankton Research*, 37, 862-868, 10.1093/plankt/fbv054, 2015.
- 840 Archibald, K. M., Dutkiewicz, S., Laufkotter, C., and Moeller, H. V.: Thermal Responses in Global Marine Planktonic Food Webs Are Mediated by Temperature Effects on Metabolism, *Journal of Geophysical Research-Oceans*, 127, 10.1029/2022jc018932, 2022.
- Bilal, N.: Implementation of Sobol's Method of Global Sensitivity Analysis to a Compressor Simulation Model, *International Compressor Engineering Conference, Herrick Laboratories, Purdue University* 2014.
- 845 CalCOFI-Scripps-Institution-of-Oceanography and Wilkinson, J.: Measurements from CalCOFI cruises in the California Current System, including log of station information, weather, sea conditions as well as physical, chemical and biological measurements including including temperature, salinity, oxygen, density, sigma theta, phosphate, silicate, nitrite, nitrate, ammonia, chlorophyll a, integrated chlorophyll a, primary productivity, and integrated primary production. 1949 - January 2020 (ver 5) [dataset], <https://doi.org/10.6073/pasta/7f8e5d24e9b27ae695295a8ddc0809d1> 2022.
- 850 California-Current-Ecosystem-LTER and Landry, M.: Size group (pico, nano, micro) and group total carbon estimates from cell counts via epifluorescent microscopy (EPI) of heterotrophic and autotrophic plankton from CCE LTER process cruises in the California Current region, 2006 - 2016 (ver 4) [dataset], <https://doi.org/10.6073/pasta/430bc600ff16ec4853fc4d594465e1fe> 2019.
- Casey, J. R., Boiteau, R. M., Engqvist, M. K. M., Finkel, Z. V., Li, G., Liefer, J., Muller, C. L., Munoz, N., and Follows, M. J.: Basin-scale biogeography of marine phytoplankton reflects cellular-scale optimization of metabolism and physiology, *Science Advances*, 8, 10.1126/sciadv.abl4930, 2022.
- 855 DeLong, J. P., Okie, J. G., Moses, M. E., Sibly, R. M., and Brown, J. H.: Shifts in metabolic scaling, production, and efficiency across major evolutionary transitions of life, *Proceedings of the National Academy of Sciences of the United States of America*, 107, 12941-12945, 10.1073/pnas.1007783107, 2010.
- 860 Dutkiewicz, S., Boyd, P. W., and Riebesell, U.: Exploring biogeochemical and ecological redundancy in phytoplankton communities in the global ocean, *Global Change Biology*, 27, 1196-1213, 10.1111/gcb.15493, 2021.
- Eckford-Soper, L. K., Andersen, K. H., Hansen, T. F., and Canfield, D. E.: A case for an active eukaryotic marine biosphere during the Proterozoic era, *Proceedings of the National Academy of Sciences*, 119, e2122042119, doi:10.1073/pnas.2122042119, 2022.
- 865 Fennel, K., Spitz, Y. H., Letelier, R. M., Abbott, M. R., and Karl, D. M.: A deterministic model for N₂ fixation at stn. ALOHA in the subtropical North Pacific Ocean, *Deep Sea Research Part II: Topical Studies in Oceanography*, 49, 149-174, [https://doi.org/10.1016/S0967-0645\(01\)00098-4](https://doi.org/10.1016/S0967-0645(01)00098-4), 2001.
- Follett, C. L., Dutkiewicz, S., Ribalet, F., Zakem, E., Caron, D., Armbrust, E. V., and Follows, M. J.: Trophic interactions with heterotrophic bacteria limit the of *Prochlorococcus*, *Proceedings of the National Academy of Sciences of the United States of America*, 119, 10.1073/pnas.2110993118, 2022.
- 870 Follows, M. J., Dutkiewicz, S., Grant, S., and Chisholm, S. W.: Emergent biogeography of microbial communities in a model ocean, *Science*, 315, 1843-1846, 10.1126/science.1138544, 2007.
- Garcia, H., Weathers, K., Paver, C., Smolyar, I., Boyer, T., Locarnini, M., Zweng, M., Mishonov, A., Baranova, O., Seidov, D., and Reagan, Jr.: *World Ocean Atlas 2018. Vol. 4: Dissolved Inorganic Nutrients (phosphate, nitrate and nitrate+nitrite, silicate)*, A. Mishonov Technical Editor, 2019.
- 875 Garcia, H. E., K. Weathers, C. R. Paver, I. Smolyar, T. P. Boyer, R. A. Locarnini, M. M. Zweng, A. V. Mishonov, O. K. Baranova, D. Seidov, and J. R. Reagan: *World Ocean Atlas 2018, Volume 4: Dissolved Inorganic Nutrients (phosphate, nitrate and nitrate+nitrite, silicate)* [dataset], 2018.
- Goericke, R.: *The structure of marine phytoplankton communities – patterns, rules and mechanisms*, 2011.
- 880 Karl, D. M. and Lukas, R.: The Hawaii Ocean Time-series (HOT) program: Background, rationale and field implementation, *Deep Sea Research Part II: Topical Studies in Oceanography*, 43, 129-156, [https://doi.org/10.1016/0967-0645\(96\)00005-7](https://doi.org/10.1016/0967-0645(96)00005-7), 1996.

- Khatiwala, S.: A computational framework for simulation of biogeochemical tracers in the ocean, *Global Biogeochemical Cycles*, 21, 10.1029/2007gb002923, 2007.
- 885 Kiørboe, T. and Thomas, M. K.: Heterotrophic eukaryotes show a slow-fast continuum, not a gleaner–exploiter trade-off, *Proceedings of the National Academy of Sciences*, 117, 24893-24899, doi:10.1073/pnas.2008370117, 2020.
- Letscher, R. T. and Moore, J. K.: Preferential remineralization of dissolved organic phosphorus and non-Redfield DOM dynamics in the global ocean: Impacts on marine productivity, nitrogen fixation, and carbon export, *Global Biogeochemical Cycles*, 29, 325-340, 10.1002/2014gb004904, 2015.
- 890 Maranon, E., Cermenon, P., Latasa, M., and Tardonleke, R. D.: Temperature, resources, and phytoplankton size structure in the ocean, *Limnology and Oceanography*, 57, 1266-1278, 10.4319/lo.2012.57.5.1266, 2012.
- McKay, M. D., Beckman, R. J., and Conover, W. J.: Comparison of three methods for selecting values of input variables in the analysis of output from a computer code, *Technometrics*, 21, 239-245, 10.1080/00401706.1979.10489755, 1979.
- Moscoso, J. E., Bianchi, D., and Stewart, A. L.: Controls and characteristics of biomass quantization in size-structured planktonic ecosystem models, *Ecological Modelling*, 468, 10.1016/j.ecolmodel.2022.109907, 2022.
- 895 Nielsen, L. T. and Kiørboe, T.: Foraging trade-offs, flagellar arrangements, and flow architecture of planktonic protists, *Proceedings of the National Academy of Sciences*, 118, e2009930118, doi:10.1073/pnas.2009930118, 2021.
- Pasulka, A. L., Landry, M. R., Taniguchi, D. A. A., Taylor, A. G., and Church, M. J.: Temporal dynamics of phytoplankton and heterotrophic protists at station ALOHA, *Deep-Sea Research Part II-Topical Studies in Oceanography*, 93, 44-57, 10.1016/j.dsr2.2013.01.007, 2013.
- 900 Reinhard, C. T., Planavsky, N. J., Ward, B. A., Love, G. D., Le Hir, G., and Ridgwell, A.: The impact of marine nutrient abundance on early eukaryotic ecosystems, *Geobiology*, 18, 139-151, 10.1111/gbi.12384, 2020.
- Salguero-Gómez, R., Jones, O. R., Jongejans, E., Blomberg, S. P., Hodgson, D. J., Mbeau-Ache, C., Zuidema, P. A., de Kroon, H., and Buckley, Y. M.: Fast–slow continuum and reproductive strategies structure plant life-history variation worldwide, *Proceedings of the National Academy of Sciences*, 113, 230-235, doi:10.1073/pnas.1506215112, 2016.
- 905 Sarmiento, J. L. and Gruber, N.: *Ocean biogeochemical dynamics*, Princeton University Press 2006.
- Sauterey, B., Ward, B., Rault, J., Bowler, C., and Claessen, D.: The Implications of Eco-Evolutionary Processes for the Emergence of Marine Plankton Community Biogeography, *American Naturalist*, 190, 116-130, 10.1086/692067, 2017.
- Sauterey, B., Ward, B. A., Follows, M. J., Bowler, C., and Claessen, D.: When everything is not everywhere but species evolve: an alternative method to model adaptive properties of marine ecosystems, *Journal of Plankton Research*, 37, 28-47, 10.1093/plankt/fbu078, 2015.
- Schartau, M., Landry, M. R., and Armstrong, R. A.: Density estimation of plankton size spectra: a reanalysis of IronEx II data, *Journal of plankton research*, 32, 1167-1184, 2010.
- Serra-Pompei, C., Soudijn, F., Visser, A. W., Kiørboe, T., and Andersen, K. H.: A general size- and trait-based model of plankton communities, *Progress in Oceanography*, 189, 10.1016/j.pocean.2020.102473, 2020.
- 915 Serra-Pompei, C., Ward, B., Pinti, J. M., Visser, A. W., Kiørboe, T., and Andersen, K. H.: Linking Plankton Size Spectra and Community Composition to Carbon Export and Its Efficiency, *Global Biogeochemical Cycles*, 36, 10.1029/2021gb007275, 2022.
- Sobol, I. M.: Sensitivity analysis for nonlinear mathematical models, *Mathematical Modeling & Computational Experiment*, 1, 407-414, 1993.
- 920 Sobol, I. M.: Global sensitivity indices for nonlinear mathematical models and their Monte Carlo estimates, *Mathematics and Computers in Simulation*, 55, 271-280, [https://doi.org/10.1016/S0378-4754\(00\)00270-6](https://doi.org/10.1016/S0378-4754(00)00270-6), 2001.
- Stammer, D., Ueyoshi, K., Köhl, A., Large, W. G., Josey, S. A., and Wunsch, C.: Estimating air-sea fluxes of heat, freshwater, and momentum through global ocean data assimilation, *Journal of Geophysical Research: Oceans*, 109, <https://doi.org/10.1029/2003JC002082>, 2004.
- 925 Stein, M.: Large sample properties of simulations using latin hypercube sampling, *Technometrics*, 29, 143-151, 10.1080/00401706.1987.10488205, 1987.
- Stoecker, D. K., Gustafson, D. E., and Verity, P. G.: Micro- and mesoprotozooplankton at 140 degrees W in the equatorial Pacific: Heterotrophs and mixotrophs, *Aquatic Microbial Ecology*, 10, 273-282, 10.3354/ame010273, 1996.
- 930 Stukel, M. R., Landry, M. R., and Selph, K. E.: Nanoplankton mixotrophy in the eastern equatorial Pacific, *Deep-Sea Research Part II-Topical Studies in Oceanography*, 58, 378-386, 10.1016/j.dsr2.2010.08.016, 2011.

- Taylor, A. G. and Landry, M. R.: Phytoplankton biomass and size structure across trophic gradients in the southern California Current and adjacent ocean ecosystems, *Marine Ecology Progress Series*, 592, 1-17, 2018.
- Taylor, A. G., Landry, M. R., Selph, K. E., and Wokuluk, J. J.: Temporal and spatial patterns of microbial community biomass and composition in the Southern California Current Ecosystem, *Deep-Sea Research Part II-Topical Studies in Oceanography*, 112, 117-128, 10.1016/j.dsr2.2014.02.006, 2015.
- 935 Taylor, A. G., Landry, M. R., Selph, K. E., and Yang, E. J.: Biomass, size structure and depth distributions of the microbial community in the eastern equatorial Pacific, *Deep Sea Research Part II: Topical Studies in Oceanography*, 58, 342-357, <https://doi.org/10.1016/j.dsr2.2010.08.017>, 2011.
- 940 Taylor, K. E.: Summarizing multiple aspects of model performance in a single diagram, *Journal of Geophysical Research-Atmospheres*, 106, 7183-7192, 10.1029/2000jd900719, 2001.
- Thingstad, T. F.: Elements of a theory for the mechanisms controlling abundance, diversity, and biogeochemical role of lytic bacterial viruses in aquatic systems, *Limnology and Oceanography*, 45, 1320-1328, <https://doi.org/10.4319/lo.2000.45.6.1320>, 2000.
- 945 Ward, B. A. and Follows, M. J.: Marine mixotrophy increases trophic transfer efficiency, mean organism size, and vertical carbon flux, *Proceedings of the National Academy of Sciences of the United States of America*, 113, 2958-2963, 10.1073/pnas.1517118113, 2016.
- Ward, B. A., Dutkiewicz, S., and Follows, M. J.: Modelling spatial and temporal patterns in size-structured marine plankton communities: top-down and bottom-up controls, *Journal of Plankton Research*, 36, 31-47, 2014.
- 950 Ward, B. A., Collins, S., Dutkiewicz, S., Gibbs, S., Bown, P., Ridgwell, A., Sauterey, B., Wilson, J. D., and Oeschlies, A.: Considering the Role of Adaptive Evolution in Models of the Ocean and Climate System, *Journal of Advances in Modeling Earth Systems*, 11, 3343-3361, 10.1029/2018ms001452, 2019.
- Wilson, J. D., Monteiro, F. M., Schmidt, D. N., Ward, B. A., and Ridgwell, A.: Linking Marine Plankton Ecosystems and Climate: A New Modeling Approach to the Warm Early Eocene Climate, *Paleoceanography and Paleoclimatology*, 33, 1439-1452, 10.1029/2018pa003374, 2018.
- 955 Winter, C., Bouvier, T., Weinbauer, M. G., and Thingstad, T. F.: Trade-Offs between Competition and Defense Specialists among Unicellular Planktonic Organisms: the “Killing the Winner” Hypothesis Revisited, *Microbiology and Molecular Biology Reviews*, 74, 42-57, doi:10.1128/mubr.00034-09, 2010.
- Wu, Z., Aharonovich, D., Roth-Rosenberg, D., Weissberg, O., Luzzatto-Knaan, T., Vogts, A., Zoccarato, L., Eigemann, F., Grossart, H. P., Voss, M., Follows, M. J., and Sher, D.: Single-cell measurements and modelling reveal substantial organic carbon acquisition by *Prochlorococcus*, *Nature Microbiology*, 7, 2068+, 10.1038/s41564-022-01250-5, 2022.
- 960 Zakem, E. J. and Levine, N. M.: Systematic Variation in Marine Dissolved Organic Matter Stoichiometry and Remineralization Ratios as a Function of Lability, *Global Biogeochemical Cycles*, 33, 1389-1407, 10.1029/2019gb006375, 2019.
- Zakem, E. J., Cael, B. B., and Levine, N. M.: A unified theory for organic matter accumulation, *Proceedings of the National Academy of Sciences*, 118, e2016896118, doi:10.1073/pnas.2016896118, 2021.
- 965 Zakem, E. J., Polz, M. F., and Follows, M. J.: Redox-informed models of global biogeochemical cycles, *Nature Communications*, 11, 10.1038/s41467-020-19454-w, 2020a.
- Zakem, E. J., Mahadevan, A., Lauderdale, J. M., and Follows, M. J.: Stable aerobic and anaerobic coexistence in anoxic marine zones, *ISME Journal*, 14, 288-301, 10.1038/s41396-019-0523-8, 2020b.
- 970 Zhou, X. and Lin, H.: Sensitivity Analysis, in: *Encyclopedia of GIS*, edited by: Shekhar, S., and Xiong, H., Springer US, Boston, MA, 1046-1048, 10.1007/978-0-387-35973-1_1191, 2008.

Supplement for “The unicellular NUM v.0.91: A trait-based plankton model evaluated in two contrasting biogeographic provinces.”

Table of Contents

S 1.	The Nutrient-Unicellular-Multicellular model	1
S 1.1.	Generalists	2
S 1.2.	Nutrients and DOC	5
S 1.3.	POM	6
S 1.4.	Water-column routine.....	6
S 2.	Inter-annual statistical variations in the dataset from CCE and Station ALOHA.....	7
S 3.	Statistics for best model solutions.....	8
S 4.	Local sensitivity analysis for CCE.....	9
S 5.	Setting up Sobol’s sensitivity assessment simulations and calculating sensitivity index.....	11
S 6.	Checking stability of Total Sobol’s sensitivity index.....	13
S 7.	Random Parameters study for Station ALOHA	14

S 1. The Nutrient-Unicellular-Multicellular model

The Nutrient-Unicellular-Multicellular (NUM) model is a modular framework comprising four separate modules: (i) the Generalist module for unicellular organisms, (ii) a specialized module for unicellular diatoms that require silica, (iii) a module for multicellular organisms, exemplified by the copepod, and (iv) a module for handling particulate organic matter (POM). The NUM model utilizes dissolved organic carbon (DOC) and a non-specific nutrient (N). Silica is included when the diatom module is employed.

In this article, we describe and evaluate the Generalist (i) and POM (iv) modules of the NUM model. The model formulations are based on Andersen and Visser (2023), who provide an in-depth explanation of the underlying motivations, which we will not reiterate here. We highly recommend interested readers refer to their comprehensive explanation.

The following sections detail the formulations for the unicellular generalist, nutrient, and DOC interactions, along with the POM module and the water-column implementation within the NUM framework. All parameters and units are listed in Table 1 of the main text.

S 1.1. Generalists

The unicellular module of the NUM model is described as a series of N unicellular organisms differing only in their size. The size classes are logarithmic distributed with geometric mean mass m_i for size group i . The energy growth rate (day^{-1}) of the generalist biomass B in size group i is described by the following equation:

$$\frac{dB_i}{dt} = g(m_i)B_i - \mu(m_i)B_i, \quad (1)$$

In this equation, $g(m_i)$ represents the synthesis rate of carbon and nitrogen (day^{-1}), and $\mu(m_i)$ represents the total mortality losses (day^{-1}). The specific forms of $g(m_i)$ and $\mu(m_i)$ are detailed below.

S 1.1.1. Synthesis rate, $g(m_i)$

The synthesis rate g of size group i is described by a type II functional response (Holling, 1959):

$$g(m_i) = j_{\max,i} \frac{J_{\text{net},i}}{J_{\text{net},i} + J_{\max,i}}, \quad (2)$$

Here, the maximum synthesis rate j_{\max} is given by:

$$j_{\max,i} = \alpha_{\max}(1 - \nu)m_i\psi, \quad (3)$$

where α_{\max} is the maximum synthesis coefficient (day^{-1}) and ν is the fraction of the cell used by cell membrane and wall, defined as $\nu = 3(\delta/r)$ with δ being the thickness of the cell wall in nm. ψ represents the temperature adjustment factor with a Q10 value of 2 (Eppley, 1971).

$J_{\text{net},i}$ is the minimum of the combined net uptake of carbon and nutrients from different sources, determined by Liebig's law of the minimum:

$$J_{\text{net},i} = \min\{j_{\text{Cnet},i}, j_{\text{Nnet},i}\} \quad (4)$$

The unicellular generalist can take up carbon as dissolved organic carbon (DOC) through osmotrophy (j_{DOC}), phototrophy (j_L), and phagotrophy (j_F), while losing carbon through respiration (j_R) and passive losses (j_{passive})

$$j_{\text{Cnet},i} = j_{\text{DOC}} + j_L + j_F - j_R - j_{\text{passive}} \quad (5)$$

Similarly, the net uptake of nutrients for the unicellular generalist involves diffusive uptake through osmotrophy (j_N) and phagotrophic uptake (j_F), with losses occurring passively (j_{passive})

$$j_{\text{Nnet},i} = j_N + j_F - j_{\text{passive}} \quad (6)$$

The uptake rates from the resources DOC ($j_{\text{DOC},i}$), light ($j_{\text{L},i}$), and nutrients ($j_{\text{N},i}$) depend on the mass-specific affinity for the given resource a_x (volume/day/gC), the concentration of the resource X (X/volume), and the Carbon: X ratio $\rho_{\text{C}:X}$ (gC/gX)

$$j_{X,i} = a_{x,i} X \rho_{\text{C}:X} \quad (7)$$

In the model a_x take the form of a_D , the mass-specific affinity for the diffusive uptake of carbon and nutrient, a_L the mass-specific affinity for carbon uptake through photosynthesis, and a_F the mass-specific affinity for phagotrophic uptake of food. The mass-specific affinities are central to the NUM model, as they account for the differences among generalist organisms that vary only in size. The affinities are thoroughly discussed in Andersen and Visser (2023) with a comprehensive presentation of model's underlying principles. Here only in short, we present the mass-specific affinity functions.

The mass-specific affinity for the diffusive uptake of carbon and nutrients a_D is described as:

$$a_D = \alpha_D r^{-2} \frac{1}{1 + \frac{r}{r_D^*}} \psi, \quad (8)$$

where α_D is the diffusive affinity coefficient, r_D^* is the diffusive affinity crossover and r is the radius of the cell.

The mass-specific affinity for carbon uptake through photosynthesis a_L is give as:

$$a_L = \varepsilon_L \frac{\alpha_L}{r} \left(1 - e^{-\frac{r}{r_L^*}} \right) m(1 - \nu), \quad (9)$$

Where α_L is the light affinity coefficient, r_L^* is the light affinity crossover and ε_L is the light uptake efficiency.

The uptake rate of phagotrophy has a constant mass-specific affinity, corresponding to the phagotrophic clearance rate. However, the actual food consumption is limited by assimilation, and the phagotrophic uptake rate is thus given by:

$$j_F = \varepsilon_F \frac{c_F}{r} \frac{a_F F}{a_F F + \frac{c_F}{r}}, \quad (10)$$

Where c_F is the maximum phagotrophic coefficient, a_F is the phagotrophic clearance rate, ε_F is the phagotrophic efficiency, and F is the amount of available food. The available food F_i is the sum of the prey in each size group j :

$$F_i = \sum_j \varphi_{ij} B_i \quad (11)$$

φ_{ij} is the size preference for predation. Predation occur when larger cells predate on smaller cells. This interaction is described as a log-normal size function that, when integrated across all size groups, has the detailed formulation:

$$\varphi_{ij} = \frac{\sqrt{\Delta}}{(\Delta - 1)\log(\Delta)} \left[\left(\frac{1}{2}s \left(e^{-\frac{\log^2(\frac{\Delta z}{\beta})}{s}} + e^{-\frac{\log^2(\frac{\Delta \beta}{z})}{s}} - 2e^{-\frac{\log^2(\frac{z}{\beta})}{s}} \right) \right. \right. \tag{12}$$

$$\left. \left. - \frac{1}{2}\sqrt{\pi}\sqrt{s} \left(\log\left(\frac{\Delta z}{\beta}\right) \operatorname{erf}\left(\frac{\log(\beta) - \log(\Delta z)}{\sqrt{s}}\right) \right. \right. \right.$$

$$\left. \left. + \log\left(\frac{\beta \Delta}{z}\right) \operatorname{erf}\left(\frac{\log(z) - \log(\Delta \beta)}{\sqrt{s}}\right) + \log\left(\frac{z}{\beta}\right) \operatorname{erf}\left(\frac{\log\left(\frac{z}{\beta}\right)}{\sqrt{s}}\right) \right) \right]$$

where $s = 2\sigma^2$, σ is the predator-prey width ratio, β is the predator-prey mass ratio, $z = \frac{m_i}{m_j}$, and $\Delta = m_i^+ / m_i^-$.

In addition to these gains, J_{net} also includes losses from respiration and passive leakages. Respiration is modeled as a constant fraction α_R of maximum synthesis:

$$j_R = \alpha_R \alpha_{\text{max}} \psi \tag{13}$$

Finally, passive leakage of nitrogen and carbon from the cell is defined as:

$$j_{\text{passive}} = \frac{c_{\text{passive}}}{r} m, \tag{14}$$

where c_{passive} is the passive loss coefficient.

S 1.1.2. Mortality losses, $\mu(m_i)$

The mortality losses for the unicellular generalist $\mu(d^{-1})$ arise from three different processes: (i) background mortality (μ_v), (ii) predation mortality from unicellular organisms (μ_p), and (iii) predation from higher trophic levels (μ_{htl}):

$$\mu(m_i) = \mu_{v,i} + \mu_{p,i} + \mu_{\text{htl},i} \tag{15}$$

The background mortality (d^{-1}) is modelled as viral lysis, assumed to be proportional to the biomass and dependent on the viral lysis mortality coefficient μ_{v0} :

$$\mu_{v,i} = \frac{\mu_{v0}}{\log\left(\frac{m_i^+}{m_{i-1}^+}\right)} B_i \tag{16}$$

The predation mortality represents internal phagotrophy within the unicellular module, where larger cells consume smaller cells. It is defined by:

$$\mu_{p,i} = \sum_i \frac{\tilde{J}_{F,i} \varphi_{ij}}{F_i} B_i \tag{17}$$

Where φ_{ij} is calculated as in equation (12), and $\tilde{J}_{F,i}$ is the down-regulated phagotrophic uptake rate after leakage of surplus nutrients:

$$\tilde{j}_{F,i} = \max\{0, j_{F,i} - (J_{\text{net},i} - g_i)\} \quad (18)$$

The higher trophic level mortality is modelled as:

$$\mu_{\text{htl}} = \mu_{\text{htl},0} \frac{1}{1 + \left(\frac{m_i}{m_{\text{htl}}}\right)^{-2}} \quad (19)$$

Where $\mu_{\text{htl},0}$ defines the size of the higher trophic level mortality and m_{htl} defines the lower size limit of the higher trophic level mortality.

S 1.2. Nutrients and DOC

Nutrients and DOC are updated several times depending on the number of modules used. Within the unicellular module, nutrients and DOC are utilized by the generalist and returned into the environment through several processes: passive losses (j_{passive}), nutrient surplus leaking from the cell ($j_{\text{Nliebig}}, j_{\text{Cliebig}}$) feeding losses (j_{feeding}), along with the fraction of background and higher-trophic level mortality that it not transferred into POM (controlled by the parameters γ_2 and γ_{ntl}).

The nutrient dynamics is described by:

$$\frac{dN}{dt} = \sum_i \left(\frac{-j_{\text{N},i} + j_{\text{passive},i} + j_{\text{Nliebig},i} + j_{\text{feeding},i}}{m_i} + \mu_{v,i}\gamma_2 + \mu_{\text{htl}}\gamma_{\text{htl}} \right) \frac{B_i}{\rho_{\text{C:N}}} \quad (20)$$

The DOC dynamics are described by:

$$\frac{d\text{DOC}}{dt} = \sum_i \left(\frac{-j_{\text{DOC},i} + j_{\text{passive},i} + j_{\text{Cliebig},i} + j_{\text{feeding},i}\gamma_F + j_{\text{photouptake},i}}{m_i} + \mu_{v,i}\gamma_2 \right) B_i \quad (21)$$

Here, the surplus of nutrient and carbon is calculated as:

$$j_{\text{Nliebig},i} = \max\{0, \tilde{j}_{\text{N},\text{net},i} - g_i\} \quad (22)$$

$$j_{\text{Cliebig},i} = \max\{0, \tilde{j}_{\text{C},\text{net},i} - g_i\} \quad (23)$$

The downregulated uptake of carbon and nutrients are described as:

$$\tilde{J}_{\text{N},\text{net},i} = j_{\text{N}} + \tilde{J}_{\text{F}} - j_{\text{passive}} \quad (24)$$

$$\tilde{J}_{\text{C},\text{net},i} = \tilde{J}_{\text{L},i} + j_{\text{DOC}} + \tilde{J}_{\text{F}} - j_{\text{R}} - j_{\text{passive}} \quad (25)$$

and

$$\tilde{J}_{\text{L},i} = j_{\text{L}} - \max\{0, \min\{j_{\text{C},\text{net}} - (j_{\text{F}} - \tilde{J}_{\text{F}}) - g\}, j_{\text{L}}\} \quad (26)$$

Finally, feeding losses and photo-uptake are described as:

$$j_{\text{feeding},i} = \frac{1 - \epsilon_F}{\epsilon_F} \tilde{J}_{\text{F},i} \quad (27)$$

$$j_{\text{photouptake},i} = \frac{1 - \epsilon_L}{\epsilon_L} \tilde{J}_{L,i} \quad (28)$$

S 1.3. POM

The NUM model handles particulate organic matter (POM) similarly to how it manages unicellular organisms. POM is divided into M logarithmic size classes, each with a geometric mean mass m_k for POM group k . The sources of POM include: (i) Mortality from higher trophic levels, (ii) feeding losses, and (iii) background mortality, while losses occur through remineralization and predation by larger cells. The assignment of background mortality to specific POM classes is described by the matrix θ . Viral lysis products are directed into the POM class closest in size to the original generalist size from which they originated, with a constraint preventing them from exceeding the original generalist size. The matrix θ contains 0s and 1s, indicating where the biomass from different sources is allocated within the POM size classes. The dynamics of POM are described by the equation:

$$\frac{d\text{POM}_k}{dt} = \sum_i (1 - \gamma_2) \mu_{v,i} \theta_{k,i} B_i + \sum_i (1 - \gamma_{htl}) \mu_{htl} \Delta_k \frac{B_i}{\rho_{C:N}} - \gamma_{\text{POM},k} P_k - \mu_{p,k} P_k \quad (29)$$

Here, $\Delta_k = \begin{cases} 0, & k < M \\ x, & k = M \end{cases}$ denotes that POM from higher-trophic level mortality is transported into the largest POM size class. $\mu_{p,k}$ describes feeding of large unicellular organisms on POM and is calculated as in equation (17). Remineralization of POM is described as

$$\gamma_{\text{POM},k} = w_k a \psi \quad (30)$$

Where w_k is the mass-specific sinking velocity described by $w_k = v_1 m_k^{v_2}$ in meters/day and a is the inverse solubilization length scale with units of m^{-1} .

Nutrients are updated as POM is remineralized back into nitrogen (N) and dissolved organic carbon (DOC):

$$\frac{dN}{dt} = \left(\frac{dN}{dt} \right)_{\text{generalist}} + \sum_k \frac{\gamma_{\text{POM}} P_k}{\rho_{C:N}} \quad (31)$$

$$\frac{d\text{DOC}}{dt} = \left(\frac{d\text{DOC}}{dt} \right)_{\text{generalist}} + \sum_k \gamma_{\text{POM}} P_k \quad (32)$$

S 1.4. Water-column routine

The water-column dynamics (mixing and sinking) is described with a transport matrix:

$$\mathbf{u}_{t+1} = (\mathbf{T}_t + \mathbf{S}) \mathbf{u}_t, \quad (33)$$

Where \mathbf{u}_t is the state vector at time t comprising nutrients, biomasses, and POM state variables, \mathbf{T}_t is the transport matrix, and \mathbf{S} is the sinking matrix. The transport matrix represents vertical mixing and is

extracted as the implicit matrix from the global 1° transport matrix MITgcm_ECCO (Stammer et al., 2004) at the two study sites on a monthly basis. The sinking matrix S represents sinking of POM as described with a first-order implicit down-wind scheme. The time step of transport and sinking is 0.5 days. In between each transport time step the ecological and biogeochemical model is integrated with a Euler scheme with a time step of 0.1 days. The boundary at the surface is closed for all state variables. The boundary at the bottom is fixed to the initial concentrations for nutrient state variables, closed for unicellular state variables, and open for sinking POM.

The light availability in the water column is dependent on the light attenuation (k_w and k_{POM}), which result from shading and scattering by dissolved and particulate organic matter in the water column. k_w is calculated based on observations at CEE. We have fitted an exponential function to observed irradiance as function of depth using the particulate organic matter concentration for each station at each measuring day in the CCE-LTER program. This has resulted in a k_{POM} value of 3×10^{-5} ($m^2 mg C^{-1}$) used here.

S 2. Inter-annual statistical variations in the dataset from CCE and Station ALOHA

In the article we compare the model result to the mean size spectrum for California Current Ecosystem (CCE) and Station ALOHA in the years 2004-2011. To evaluate the model results we compare the deviations from the mean observations with the inter-annual variability in Root-Mean-Squared-difference ($RMSd_{iao}$), Standard Deviation (STD_{iao}) and Correlation coefficient (COR_{iao}) given in Table S1.

Table S2.1: The Root-Mean-Squared-difference, Standard Deviation and Correlation between annual observation versus mean of year 2004-2001 for CCE ($RMSd_{iao}$, STD_{iao} , and COR_{iao})

CCE	B _{T-pico}	B _{T-nano}	B _{A-pico}	B _{A-nano}	B _{A-micro}
$RMSd_{iao}$	0.4	0.3	2.7	0.4	1.0
STD_{iao}	2	1.4	2.1	1.4	1.4
COR_{iao}	0.2	0.7	0	0.7	0.96
Station ALOHA	B _{T-pico}	B _{T-nano}	B _{A-pico}	B _{A-nano}	B _{A-micro}
$RMSd_{iao}$	0.04	0.5	0.2	0.4	1.0
STD_{iao}	1.2	1.6	1.4	1.5	2.6
COR_{iao}	0.97	0.9	0.96	0.9	0.7

S 3. Statistics for best model solutions

Model Root-Mean-Squared-difference ($RMSd_{m-o}$), and Correlation coefficient (COR_{m-o}) for the best model fit to observations.

Table S2: The Root-Mean-Squared-difference, and Correlation between model result and mean of year 2004-2001 for CCE ($RMSd_{m-o}$, and COR_{m-o}) for the best parameter combinations for CCE. Compare with Table S1 for boundaries. Values highlighted with grey are not within the inter-annual variability of the observations.

simulation nr.		CCE				
		B _{T-pico}	B _{T-nano}	B _{A-pico}	B _{A-nano}	B _{A-micro}
		RMSd _{m-o}				
RMSd _{m-o}	1703	0.64	0.60	0.08	0.25	0.40
	5801	0.48	0.71	0.05	0.39	0.51
	39986	0.57	0.45	0.16	0.19	0.23
	41402	0.53	0.37	0.13	0.22	0.67
	49833	0.63	0.40	0.19	0.17	0.35
	91224	0.54	0.47	0.08	0.22	0.27
	99032	0.55	0.50	0.10	0.32	0.67
		COR _{m-o}				
COR _{m-o}	1703	0.86	0.96	0.98	0.98	0.89
	5801	0.83	0.98	0.98	0.99	0.90
	39986	0.98	0.94	1.00	0.96	0.95
	41402	0.93	0.96	1.00	0.98	0.79
	49833	0.93	0.95	1.00	0.97	0.91
	91224	0.95	0.94	0.99	0.96	0.92
	99032	0.93	0.97	0.98	0.99	0.80

Table S3: The Root-Mean-Squared-difference, and Correlation between model result and mean of year 2004-2001 for CCE ($RMSd_{m-o}$, and COR_{m-o}) for the best parameter combinations for CCE. Compare with Table S1 for boundaries. Values highlighted with grey are not within the inter-annual variability of the observations.

		Station ALOHA				
		B_{T-pico}	B_{T-nano}	B_{A-pico}	B_{A-nano}	$B_{A-micro}$
simulation nr.		$RMSd_{m-o}$				
$RMSd_{m-o}$	29534	0.17	0.56	0.09	0.12	0.88
	37705	0.31	1.08	0.29	0.36	1.69
	69585	0.12	0.67	0.13	0.20	1.29
	74294	0.41	1.18	0.24	0.18	2.77
		COR_{m-o}				
COR_{m-o}	29534	0.97	0.97	0.99	0.99	0.78
	37705	0.98	0.90	0.97	0.95	0.72
	69585	0.96	0.96	0.97	0.99	0.71
	74294	1.00	0.95	0.98	0.99	0.81

S 4. Local sensitivity analysis for CCE

The aim of the local sensitivity assessment is to evaluate each parameter's effect on the model result. The range of each free parameter is based on the range defined by the solutions with optimal fit (Fig. 6). Several of the parameters result in a threshold sensitivity (systems bifurcation point) where the model solution changes abruptly. We note as an example the threshold sensitivity related to the phagotrophic assimilation rate (ϵ_F), where there is an abrupt increase in microplankton at $\epsilon_F \sim 0.25$ (Fig. S1a). ϵ_F has a highly non-linear effect on the ecosystem expressed in terms of light harvesting and food consumption (Fig. S1b,c). As ϵ_F decrease, the bifurcation in the ecosystem is associated with an abrupt reduction of food consumption in the lower half of the phytoplankton mass (size) spectrum, resulting in lower overall biomass, a reduction of light harvesting as a result of more unassimilated food is shunted into DOC and shading. While being extremely interesting, the detailed analysis of such bifurcation points is beyond the current scope and remains a prospect for future analyses.

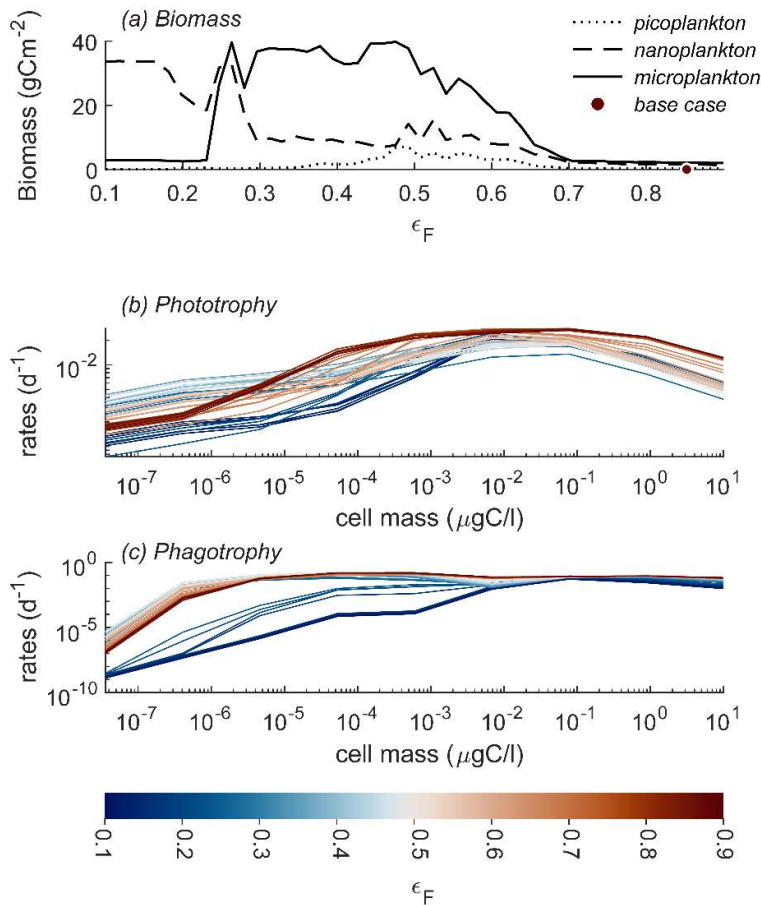


Figure S1: Model threshold sensitivity related to the phagotrophic assimilation rate (ϵ_F) with an abrupt decrease in microplankton as ϵ_F decrease below ~ 0.25 (a). Note how this bifurcation point behavior is associated with light harvesting (b); light harvesting initially decreases for nearly all cell mass as ϵ_F decrease, but suddenly at ~ 0.25 results in a significant reduction mainly in the lower half of the mass range. Phagotrophic food consumption also suddenly decreases at ~ 0.25 (c). Model parameter combination is Test 41402, with local sensitivity plot shown in Fig. S2

Overall, the random sampling of the restricted parameter span, as well as local sensitivity study show that most parameters are highly coupled in term of ecosystem sensitivity, where the effect of individual parameters are intertwined and result in a highly non-linear system. An illustration of this non-linearity can be seen by comparing the local sensitivity of two of our nine optimal fits. The two sets of local sensitivity analyses result in very different estimates of the parameter sensitivity (Fig. S2). One model, with its initial optimal parameter set, yielded nearly equally sensitive to almost all parameters with only a_F , σ and m_{HTL} standing out in RMSd (Fig. S2a). In contrast, ϵ_F is the absolute most important parameter in the other model (Fig. S2b).

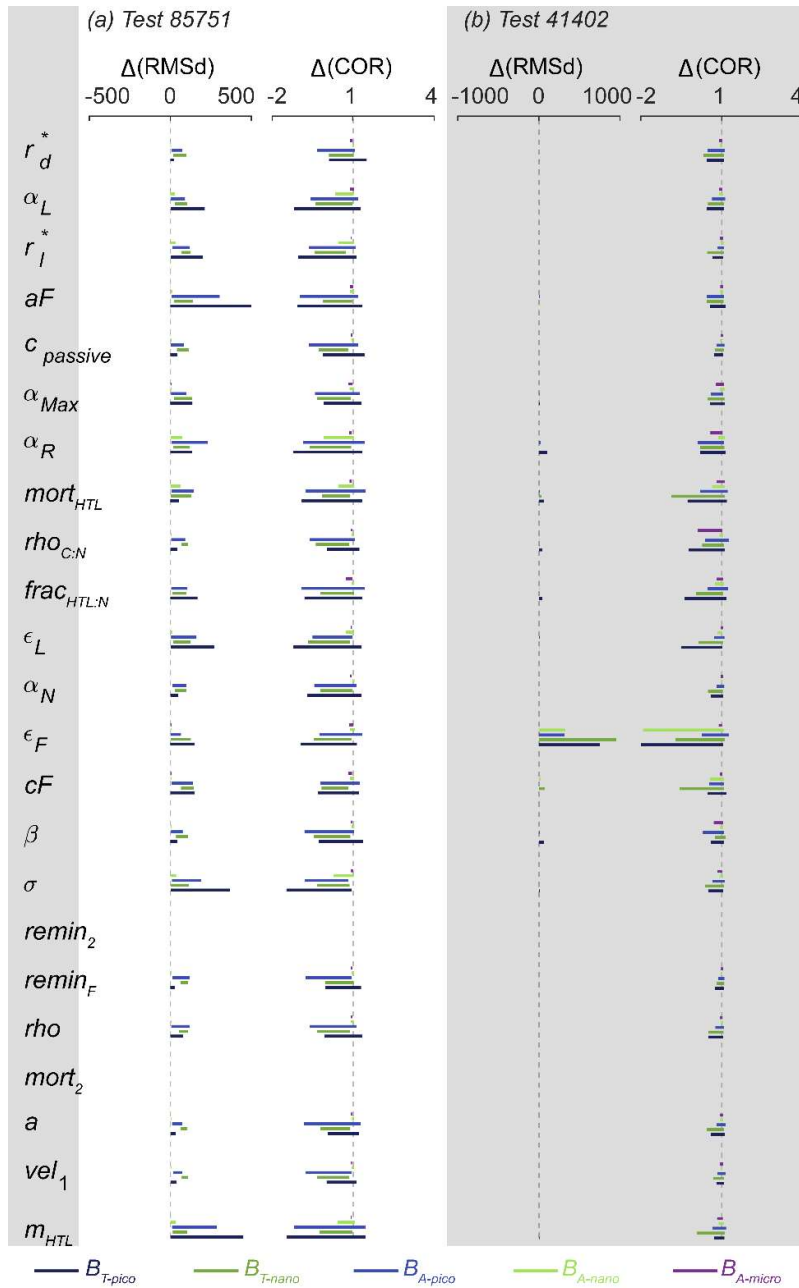


Figure S2: Local sensitivity, for two optimal model results, where only one parameter is varied at the time. The variation is within the restricted parameter span based on the parameter range for the nine statistically optimal parameter combinations for CCE. Note how model test 85751 is sensitive to change in most parameters (a) whereas model test 41402 (b) is strongly sensitive to ϵ_F . Abbreviations as in Fig. 2 and parameters in Table 1.

S5. Setting up Sobol's sensitivity assessment simulations and calculating sensitivity index

The following is a “dummy” script for setting up a Sobols Sensitivity Analysis and calculating the Sobols sensitivity index.

Step 1: Run the model with three sets of parameters:

% a. "Original": 20,000 simulations with predefined Latin Hypercube Sampling of random parameters in a 23-parameter space.

% b. "Set 1": 460,000 simulations. For each of the 20,000 original simulations, run 23 simulations where each parameter is held at its "original" value while changing all other parameters within the same parameter space as the original collection.

% c. "Set 2": 460,000 simulations where each parameter is varied individually while the other parameters are held constant at their "original" values.

Step 2: Sorting data:

% a. The result of simulations in 1a becomes a column vector from 1 to 20,000, called "y0."

% b. The result of simulations in 1b becomes a matrix that is 23 times 20,000 in size, where row 1 corresponds to simulations where parameter 1 is held at its "original" value while all others are varied (and so on for all 23 rows/parameters). This matrix is called "y1."

% c. The result of simulations in 1c becomes a matrix that is 23 times 20,000 in size, where row 1 corresponds to simulations where only parameter 1 is varied while others are held at their "original" values (and so on for all 23 rows/parameters). This matrix is called "y2."

Step 3: Calculate f0 and D using the formula:

```
f0 = sum(y0)/20000;
```

```
D = sum(y0.^2)/20000;
```

```
D = D - f0.^2;
```

Step 4: Calculate Di and Di_tot using the formula:

```
Di = ones(23, 1) * D;
```

```
Ditot = zeros(23, 1);
```

```
for i = 1:20000
```

```
    for j = 1:23
```

```
        Di(j) = Di(j) - (y0(i) - y1(j, i)).^2 / (2 * 20000);
```

```
        Ditot(j) = Ditot(j) + (y0(i) - y2(j, i)).^2 / (2 * 20000);
```

```
    end
```

```
end
```

Step 5: Calculate the First-order (S1) and Total (St) effect sensitivity indices:

```
S1 = Di./D;
```

```
St = Ditot./D;
```

S6. Checking stability of Total Sobol's sensitivity index

To test if 20,000 random simulations is enough to assess the Sobol's Total index (STi) we evaluated the evolution of STi as a function of the number of simulations. Fig. S3 show that the STi for Root-Mean-Square difference (RMSd) for AC_{pico} is stable for most of the parameters after approximately 7,000 random simulations.

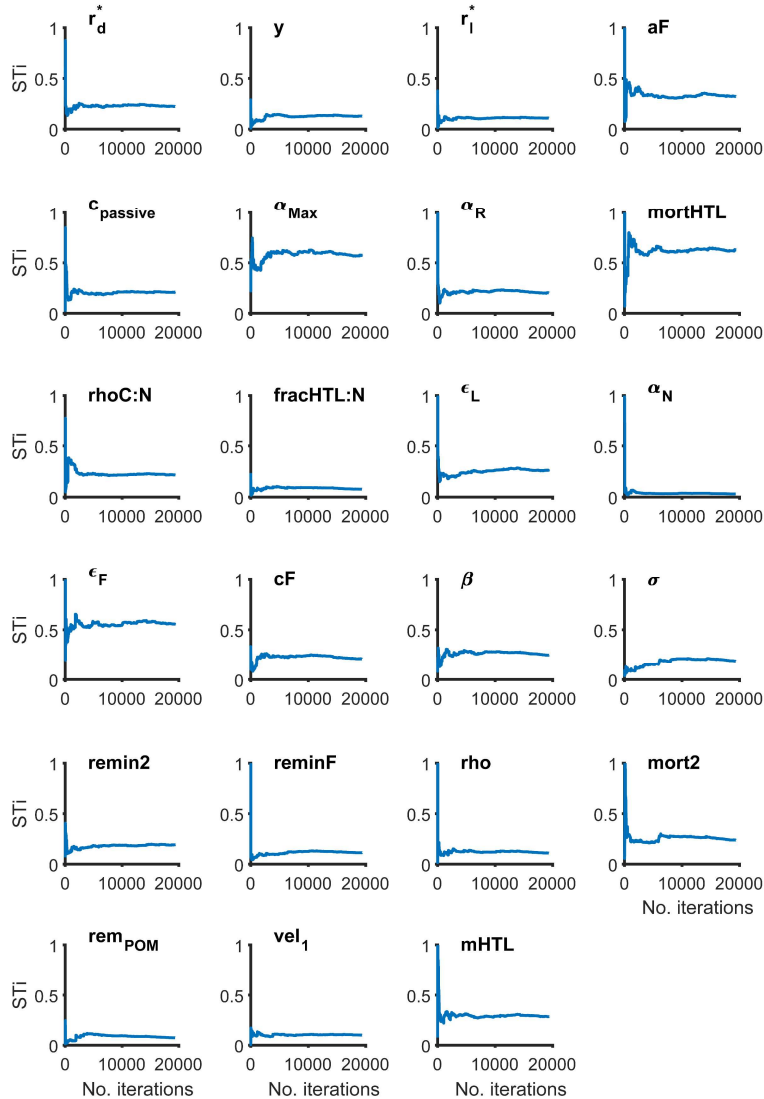


Figure S3: Sobol's Total index (STi) calculated on RMSd for AC_{pico} as a function of the number of simulations, for each of the 23 parameters. Most of the parameters show large variations with few simulations but the STi values are stable above approximately 7,000 simulations.

The manuscript includes the global parameter sensitivity ranked based on sensitivity index calculated for RMSd but not correlation which is added in Fig. S4. The result for correlations supports the result for RMSd showing a model sensitivity towards predation and synthesis.

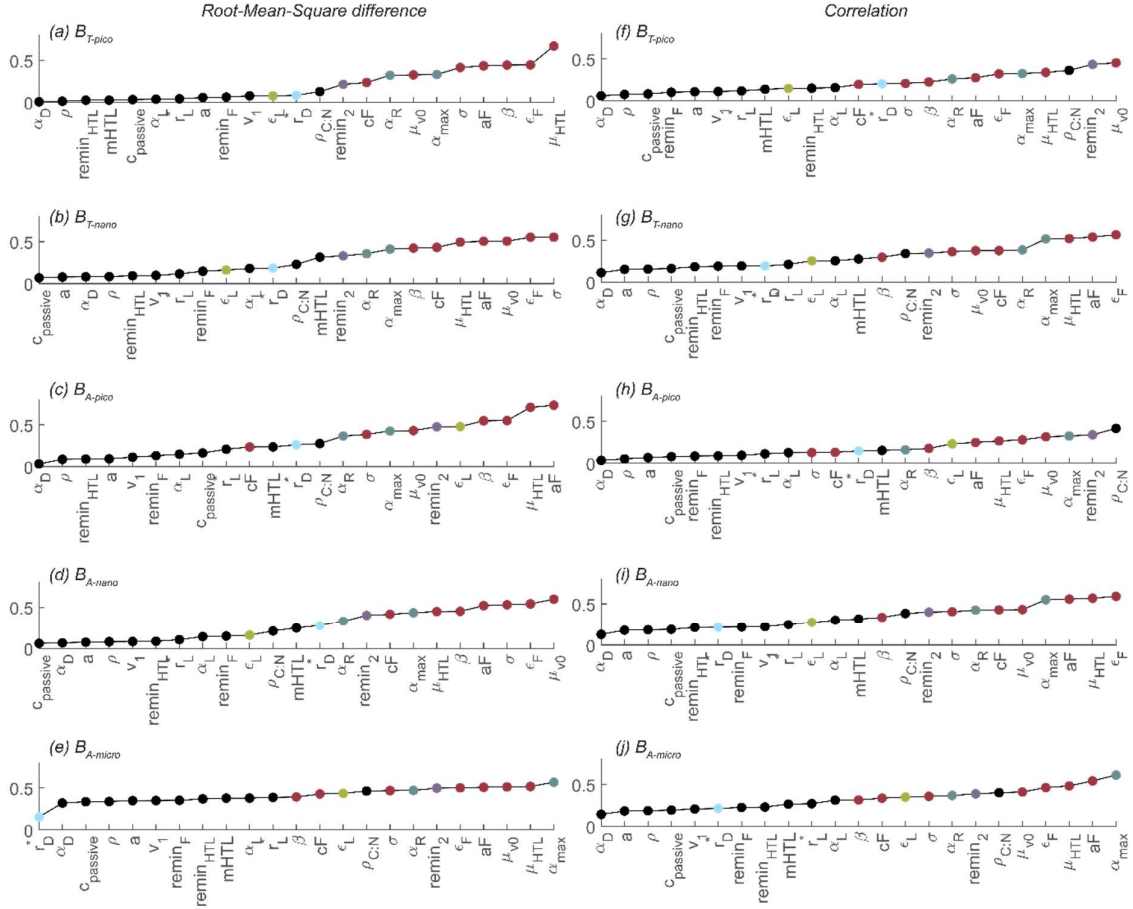
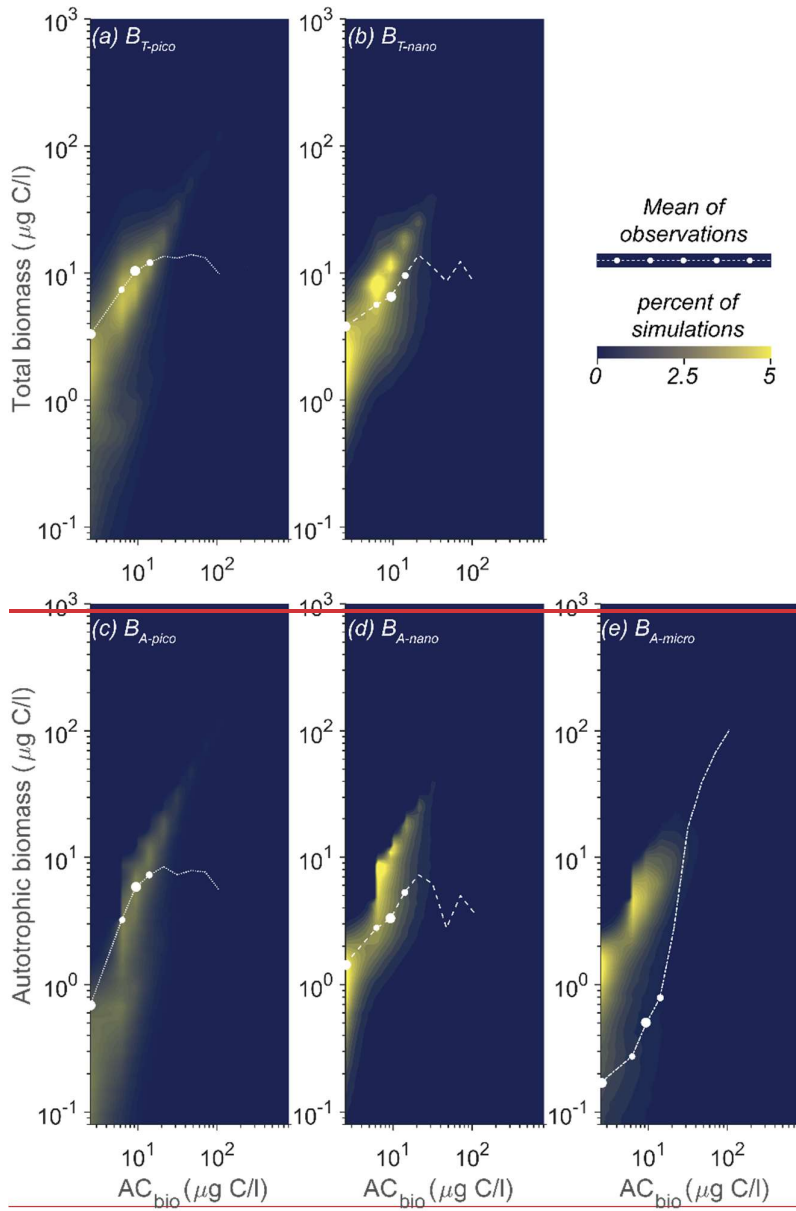


Figure S4: Global parameter sensitivity ranked based on sensitivity index calculated by Sobol's variance-based sensitivity method for non-linear models for RMSd and Correlation. Note how all biomass sizes are especially sensitive to parameters controlling predation (red dots) and synthesis (grey dots). Parameter definitions in Table 1 and other abbreviations in Fig. 2.

S7. Random Parameters study for Station ALOHA

The first order parameter sensitivity study was done for both CCE and Station ALOHA. Figure S5 below show the result for Station ALOHA. The figure shows how many of the model simulations underestimate pico- and nanoplankton at low AC_{bio} while overestimate at higher AC_{bio} . The simulations generally overestimate the microautotrophic biomass. This pattern is very similar to the pattern for the 100,000 simulations for the first-order sensitivity analysis at CCE (compare to Fig. 5 in text).



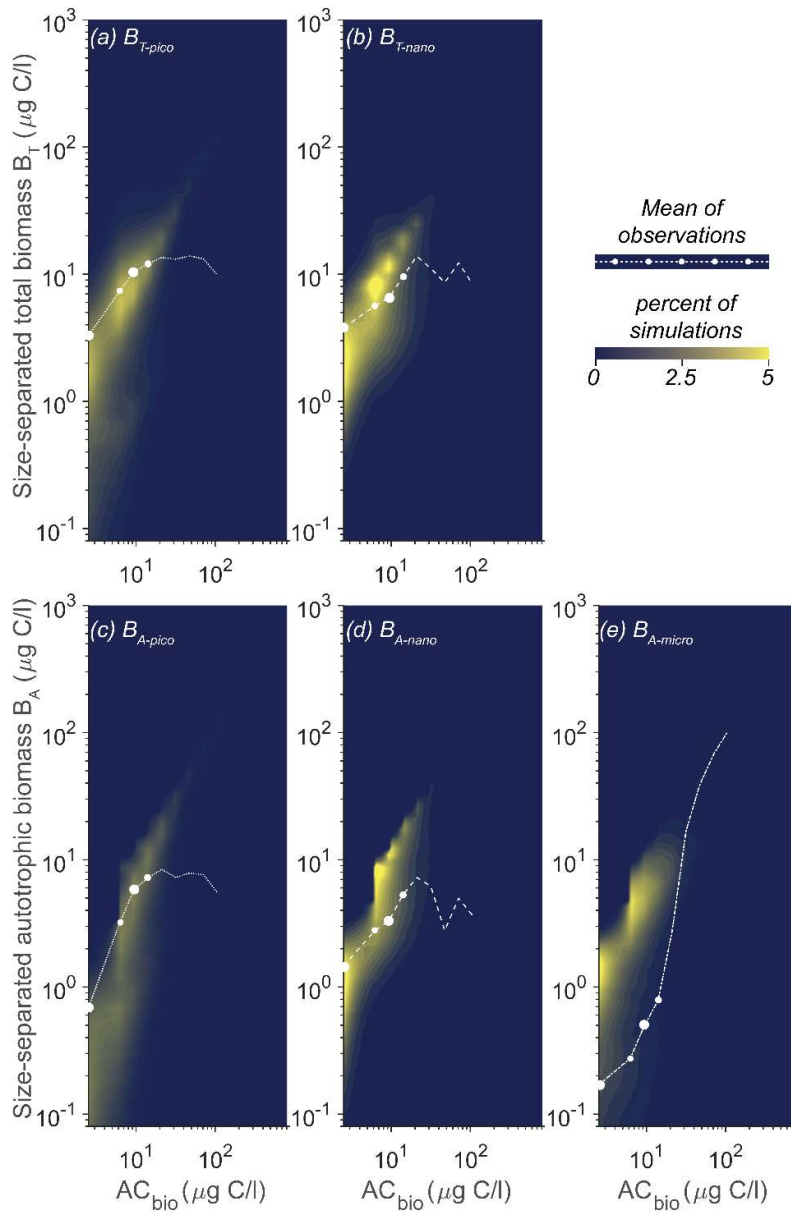


Figure S5: Model mean and total biomass of size groups as a function of total biomass for the 100,000 random parameter combinations for Station ALOHA. Black dots are observations in AC_{bio} bins. Abbreviations as Fig. 2.

References

- Andersen, K. H. and Visser, A. W.: From cell size and first principles to structure and function of unicellular plankton communities, *Progress in Oceanography*, 213, 102995, <https://doi.org/10.1016/j.pocean.2023.102995>, 2023.
- Eppley, R. W.: Temperature and phytoplankton growth in the sea, *Fishery bulletin*, 70, 1063, 1971.

Holling, C. S.: Some characteristics of simple types of predation and parasitism¹, *The Canadian Entomologist*, 91, 385-398, 1959.

Stammer, D., Ueyoshi, K., Köhl, A., Large, W. G., Josey, S. A., and Wunsch, C.: Estimating air-sea fluxes of heat, freshwater, and momentum through global ocean data assimilation, *Journal of Geophysical Research: Oceans*, 109, <https://doi.org/10.1029/2003JC002082>, 2004.